I&EC research
Industrial & Engineering Chemistry Research

pubs.acs.org/IECR
Article

Extraction, Characterization, and Stability Studies of Bistriazinyl-Derived Carboxylic Acids

Laura Diaz Gomez, Patrik Weßling, Andreas Wilden,* Petra J. Panak, Gregory P. Horne, Stephen P. Mezyk, Julie R. Peller, Andreas Geist, and Giuseppe Modolo

Cite This: *Ind. Eng. Chem. Res.* 2026, 65, 6127−6142

ABSTRACT: Separation of An(III) and Ln(III) ions will benefit the recycling of used nuclear fuel (UNF). For this purpose, many ligands have been tested over the years, and several separation processes have been successfully demonstrated on the laboratory scale. Current research aims at the development of new ligands that are built only with carbon, hydrogen, oxygen, and nitrogen (CHON), as they can be incinerated completely without secondary waste production. Here, we tested a new class of water-soluble ligands, the bistriazinyl-octa-carboxylic acids. One member, in particular, 2,6-bis-[5,6-di(3,4-dicarboxyphenyl)-1,2,4-triazin-3-yl]-pyridine (BTPOA), was found to be suitable for the selective separation of Am(III) and Cm(III) ions from Ln(III) ions and may act as a CHON alternative to its sulfonated analogue (SO_3-Ph-BTP). BTPOA exhibited good extraction results and a high selectivity for Am(III) over Eu(III) ions. This ligand's complexation of metal ions was further studied using potentiometric spectroscopy, as well as time-resolved laser-induced spectroscopy with Cm(III) and Eu(III) in aqueous $HClO_4$ and HNO_3 media. Conditional stability constants of each formed species were determined. In the $HClO_4$ system, Cm(III) formed three species (1:1, 1:2, and 1:3) through the stepwise addition of a single BTPOA molecule. On the other hand, in HNO_3, Cm(III) formed two 1:2 complexes and one 1:3 complex, while the stepwise formation of three species was observed for Eu(III). The stability constants are comparable to the values for SO_3-Ph-BTP. The radiolytic behavior of BTPOA was also investigated using electron pulse irradiation measurements to determine absolute rate coefficients (k) under ambient temperature conditions for the reaction of BTPOA with typical UNF reprocessing radical radiolysis products—the hydrated electron (e_{aq}^-, $k = (1.60 \pm 0.02) \times 10^{10}$ M^{-1} s^{-1}), the hydrogen atom ($H^\bullet$, $k = (2.17 \pm 0.03) \times 10^9$ M^{-1} s^{-1}), and hydroxyl ($^\bullet OH$, $k = (6.95 \pm 0.06) \times 10^9$ M^{-1} s^{-1}) and nitrate ($NO_3^\bullet$, $k = (0.37 \pm 0.02) \times 10^7$ M^{-1} s^{-1}) radicals. These rate coefficients indicate that the radiolytic longevity of BTPOA should increase with HNO_3 concentration, owing to the consumption of $e_{aq}^-/H^\bullet$, by nitrate anions, and the replacement of $^\bullet OH$ by the less reactive $NO_3^\bullet$.

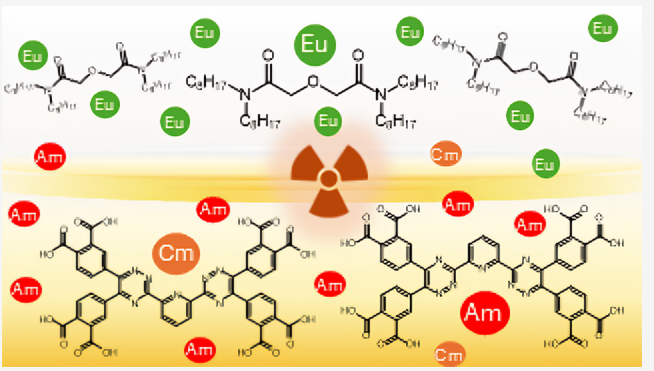

INTRODUCTION

The separation of minor actinides (An), lanthanides (Ln), and other fission products from used nuclear fuel (UNF) or plutonium uranium reduction extraction (PUREX)[1] raffinate will benefit nuclear waste management strategies by reducing the radiotoxicity and decay heat burden on long-term storage.[2,3] Am(III), Cm(III), and Ln(III) ion separation is a particularly challenging task due to their similar atomic radii and chemical properties. In the last two decades, different studies were published on the separation of An(III) from Ln(III) (GANEX and EURO-GANEX),[4−6] the coseparation of Am(III)/Cm(III) from Ln(III) (SANEX and *i*-SANEX),[7−11] and the selective separation of Am(III) from UNF (AmSel and EXAm).[12,13] These processes use solvent extraction techniques to selectively complex metal ions of interest using organic and/or water-soluble ligands.

The bistriazinyl (BTP) family are N-donor ligands that are highly selective toward An(III) over Ln(III). They have been studied as lipophilic ligands[12,14−17] and can also be modified to be hydrophilic masking agents/hold-back reagents by inclusion of sulfophenyl, hydroxyl, carboxylic acid, or other hydrophilic functional groups to the outer periphery of the BTP architecture.[14] Their structures have been refined to increase their stability in acidic media, improve selectivity, and create a synergistic extraction system by combining lipophilic and hydrophilic ligands with inverse selectivity.[18]

Received: November 17, 2025
Revised: February 18, 2026
Accepted: February 26, 2026
Published: March 13, 2026

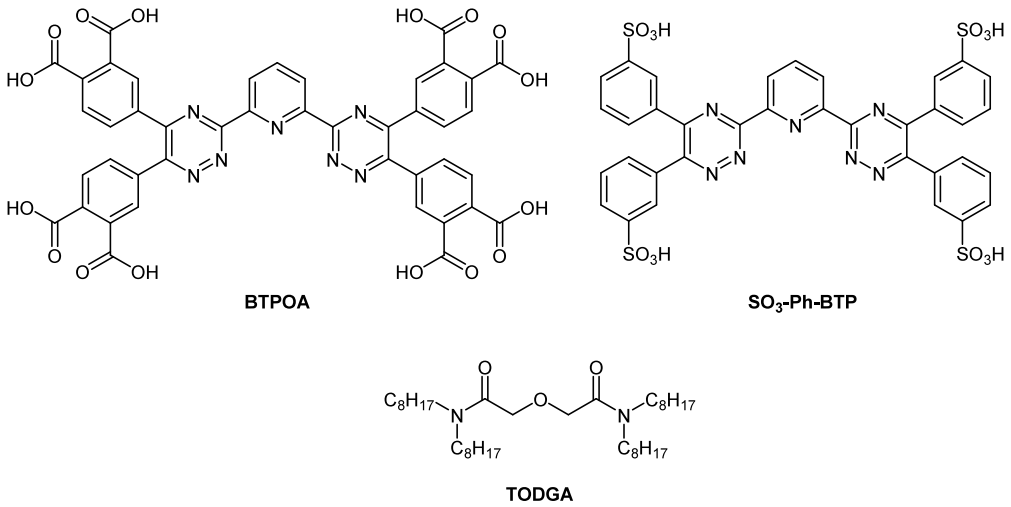

Figure 1. Molecular structures of BTPOA, SO_3-Ph-BTP, and TODGA.

For example, the *i*-SANEX[8] solvent system uses *N*,*N*,*N*′,*N*′-tetraoctyl diglycolamide (TODGA, Figure 1) in combination with SO_3-Ph-BTP[18] to produce the desired synergistic system.[14,16] The hydrophilic SO_3-Ph-BTP ligand complexes retain Am(III) and Cm(III) in the aqueous phase, allowing for the extraction of Eu(III) and other Ln(III) TODGA complexes into the organic phase. Ligands with only carbon, hydrogen, oxygen, and nitrogen in their structure (so-called CHON principle) are currently the preferred option because they can be fully incinerated without further treatment.[19] Several studies have tested a variety of CHON molecules to achieve these separation objectives.[20−22] The present study focuses on a CHON alternative to SO_3-Ph-BTP, substituting the sulfophenyl groups for carboxylic acid groups (BTPOA, Figure 1), although the impact of this substitution on separations is currently unknown.

In addition to good solubility in aqueous acidic media, another key aspect for candidate ligands under UNF reprocessing conditions is their longevity in the presence of ionizing radiation fields. Irradiation of reprocessing solvent systems typically results in the destruction of ligands and the formation of problematic degradation products, the consequences of which determine the An(III)/Ln(III) separation efficiency and solvent recyclability. The radiation chemistry of BTP molecules has been investigated in several process-relevant media, although the majority of these studies focused upon the organic phase.[23−36] In aqueous solutions, the radiolytic behavior of SO_3-Ph-BTP has been investigated.[37,38] Using a combination of experiment and multiscale modeling methods, Horne et al.[39] provided a thorough characterization of SO_3-Ph-BTP radiolysis in neat water, finding near-complete (>90%) ligand destruction within 1 kGy of absorbed gamma radiation dose, for which the oxidizing hydroxyl radical ($^{\bullet}OH$, E° = 2.7 V)[40] was shown to be predominantly responsible. Galan[37] and Peterman[38] reported greater SO_3-Ph-BTP radiolytic longevity (100s of kGy) in dilute nitric acid (HNO_3) media. Although both studies indirectly probed the extent and impacts of SO_3-Ph-BTP radiolysis using An(III)/Ln(III) distribution ratios, a basis for enhanced SO_3-Ph-BTP longevity in HNO_3 solution could be argued in terms of changes in the suite of available radiolysis products. More specifically, as the concentration of HNO_3 is increased, neat water radiolysis products (eq 1)[40] are progressively converted into HNO_3 radiolysis products (eqs 2−7):[40−46]

$$H_2O \rightsquigarrow e_{aq}^{-},\ H^{\bullet},\ {}^{\bullet}OH,\ H_2O_2,\ H_2,\ H_{aq}^{+} \quad (1)$$

$$HNO_3/NO_3^{-} \rightsquigarrow e_{aq}^{-},\ NO_3^{\bullet},\ HNO_2/NO_2^{-},\ O^{\bullet},\ H_{aq}^{+} \quad (2)$$

$$HNO_3 \rightleftharpoons NO_3^{-} + H_{aq}^{+} \quad pKa \sim -1.37 \quad (3)$$

$$e_{aq}^{-} + NO_3^{-} \rightarrow NO_3^{\bullet 2-} \xrightarrow{2Haq^{+}} (H_2O + NO_2^{\bullet}) \rightarrow \rightarrow HNO_2 \quad k = 9.7 \times 10^{9} M^{-1}s^{-1} \quad (4)$$

$$H^{\bullet} + NO_3^{-} \xrightarrow{Haq^{+}} (H_2O + NO_2^{\bullet}) \rightarrow \rightarrow HNO_2 \quad k = 5.6 \times 10^{6}\ M^{-1}s^{-1} \quad (5)$$

$$OH^{\bullet} + HNO_3 \rightarrow NO_3^{\bullet} + H_2O \quad k = 5.3 \times 10^{7}\ M^{-1}s^{-1} \quad (6)$$

$$H_2O_2 + HNO_2 \rightarrow NO_3^{\bullet} + H_2O \quad k = 1.9 \times 10^{7}\ M^{-1}s^{-1} \quad (7)$$

Most notably, the $^{\bullet}OH$ is replaced by the typically less oxidizing nitrate radical ($NO_3^{\bullet}$, E° = 2.3−2.6 V).[47] Given these changes, a greater radiolytic longevity may be expected for SO_3-Ph-BTP in HNO_3 media. That said, Kynman et al. recently showed that the radiation-induced chemical reactivity of SO_3-Ph-BTP is influenced by actinide complexation, reporting an order-of-magnitude increase in its rate of reaction with $NO_3^{\bullet}$ when complexed to Am(III).[48]

Irrespective, substitution of the solubilizing sulfophenyl functionality in SO_3-Ph-BTP for carboxylate groups will ultimately alter the BTP molecule's radiolytic behavior and, thus, its longevity under envisioned process conditions. Consequently, the interaction of BTPOA with typical UNF reprocessing radical radiolysis products—the hydrated electron (e_{aq}^{-}), the hydrogen atom ($H^{\bullet}$), $^{\bullet}OH$, and $NO_3^{\bullet}$—must be quantitatively understood to evaluate the feasibility of this ligand under real-world process conditions.

Considering the above, our goal is to evaluate the separations and radiolytic stability properties of BTPOA to assess its suitability as a replacement for SO_3-Ph-BTP in the *i*-

https://doi.org/10.1021/acs.iecr.5c04766
Ind. Eng. Chem. Res. 2026, 65, 6127−6142

SANEX or GANEX process solvent system. Here, we report stability studies for hydrolysis, radiation-induced reaction kinetics, and distribution ratio temperature dependence, as well as characterization studies, including kinetics, acid constant (pK_a) determination, and the speciation of BTPOA complexes of An(III) and Ln(III) via time-resolved laser-induced fluorescence spectroscopy (TRLFS).[49]

METHODS

Ligand Synthesis

The company is unable to disclose the synthesis route. Nevertheless, it is imperative to emphasize that the ligand was synthesized with eight carboxylic acids in the outer sphere with the objective of enhancing solubility and, consequently, the solubility factor. This is predicated on the fact that only four acids will be feasible in the salt form.

Solvent Extraction

Batch solvent extraction experiments were carried out using equal volumes of 500 μL of each phase. The aqueous and organic phases were pipetted into screw-cap glass vials and contacted for a given time on an IKA VIBRAX VXR, IKA-Werke GmbH & Co. KG (Staufen, Germany) basic automatic shaker at 2,200 rpm and 22 °C. The temperature was controlled by a F25-HE thermostat, JULABO GmbH (Seelbach, Germany). After mixing, the samples were centrifuged with a Hettich EBA 8s centrifuge, Andreas Hettich GmbH & Co.KG (Tuttlingen, Germany), for 5 min. The phases were then separated manually using a fine-tipped transfer micropipette. 200 μL of each phase was transferred into new glass vials for further analyses.

Gamma measurements of ^{241}Am (60 keV) and ^{152}Eu (122 keV) were carried out using an Eurisys EGC 35−195-R germanium coaxial N-type detector, and spectra were evaluated using the GammaVision Software. Samples were measured directly without further treatment. Alpha measurements were carried out for ^{241}Am (5486 keV) and ^{244}Cm (5805 keV) using an Ortec/Ametek ALPHA-ENSEMBLE-8 eight-chamber alpha measurement system equipped with PIPS detectors purchased from Ametek GmbH (Meerbusch, Germany). Sample preparation for alpha measurement was done by homogenizing a 10 μL alpha-spectroscopy sample in 100 μL of a mixture of Zapon varnish and acetone (1:100 v/v). This mixture was distributed over a stainless-steel plate obtained from Berthold, Bad Wildbad, Germany. The sample was dried under a heating lamp and annealed into a stainless-steel plate by a gas-flame burner. For stable elements, inductively coupled plasma mass spectrometry (ICP-MS) was applied using a PerkinElmer NexION 2000C. Aqueous samples were measured after dilution in 1% v/v HNO_3 solution without further treatment. Organic samples were measured directly in a surfactant matrix (Triton-X-100) in 0.1% v/v HNO_3 after dilution and were compared with back extraction with 0.5 M ammonium glycolate in 1% HNO_3.

Simulated High Active Raffinate (HAR)

To process the simulated PUREX raffinate solution with the proposed system, a series of steps must be carried out in a specific order. First, the feed solution is mixed with 1,2-diaminocyclohexane-*N*,*N*,*N*′,*N*′-tetracetic acid (CDTA) until a concentration of 50 mM is reached, acting as a masking agent for Pd and Zr.[1] Subsequently, the loading step is conducted by mixing the HAR + CDTA solution with 0.2 M TODGA with the objective of transferring the trivalent actinides and lanthanides to the organic phase. Afterward, the organic phase must be cleaned of any unwanted coextracted metals, a process known as scrubbing. This is achieved by mixing the loaded organic phase with 0.5 M HNO_3. This step can be repeated as necessary; however, in this case, it was performed once. Finally, the stripping step took place by combining the loaded TODGA with the aqueous phase, which contained 0.01 M BTPOA in different concentrations of HNO_3 and 10 μM of all Ln (except *Pm*).

Distribution ratios (D) were calculated as the ratio of activity or metal ion (M) concentration in the organic phase vs the activity or metal ion concentration in the aqueous phase ($[M]_{org}/[M]_{aq}$). The separation factor (SF) between two metal ions was calculated as the ratio of the corresponding distribution ratios ($SF_{M1/M2} = D_{M1}/D_{M2}$). Distribution ratios between 0.01 and 100 exhibit an uncertainty of ±5%, while lower/higher values exhibit larger uncertainties. Mass balances were calculated as the sum of the aqueous and organic concentrations divided by the initial concentration.

pK_a Determination

First, the titrator TITRANDO was calibrated by titrating 0.1 M oxalic acid with 0.1 M NaOH and 0.1 M HNO_3. Afterward, we proceeded with electrode calibration with buffer solutions of pH 1, 4, 7, 10, and 12. Known concentrations of HNO_3 and NaOH were tested. Solutions with 8 mg of BTPOA, 30 mg of BTBPOA, and 30 mg BTPhenOA were prepared and titrated with 0.1 M NaOH and 0.1 M HNO_3 to obtain the deprotonated and protonated forms of the molecules.

Another approach to keep the ionic strength constant consisted of adding $NaNO_3$ into the titrant 0.1 M NaOH. In addition, the sample was diluted in a solution of 0.1 M HNO_3 and 1.9 M $NaNO_3$ to have a final nitrate concentration of 2 M. The first trial started with a 5 mM ligand solution at pH 1 to reach the full protonation of the ligand and to stepwise deprotonate it with the titrant. The second trial, the titrant was changed to 1 M NaOH with 1 M $NaNO_3$, and the concentration of the ligand was decreased to 2.5 mM, and for the last trial, the concentration of the ligand increased to 7.5 mM. The data was analyzed using *Hyperquad 2013*.

TRLFS Titration

For these titration experiments, monophasic samples of Cm(III) and Eu(III) in the respective acidic media were prepared. For Cm(III) and Eu(III), 4.7 μL of 21.2 μM $Cm(ClO_4)_3$ and 9.4 μL of 1.07 mM $Eu(ClO_4)_3$ were dissolved in 1 mL of 1 mM $HClO_4$, resulting in stock solutions of 0.1 μM Cm and 10 μM Eu. First scoping experiments showed that the Eu concentration was too high, resulting in an overflow of the camera due to the high fluorescence intensity. Therefore, in the case of Eu, it was necessary to reduce the concentration by 2 orders of magnitude, resulting in a stock solution concentration of 0.1 μM. Aliquots of ligand solution were added stepwise, and the emission spectra were recorded after reaching chemical equilibrium for each step. For the Cm-nitrate system, the laser energy was reduced with the objective of avoiding any compromise to the structure of the ligand or complex.

RESULTS AND DISCUSSION

Solubility

The initial step in characterizing these compounds and assessing their potential use in solvent extraction is to evaluate their solubility in aqueous HNO_3, as this is used as the aqueous phase in the conventional PUREX process. All three ligands are soluble in water at concentrations of up to 0.1 M. In HNO_3, their solubility decreases as the concentration of acid increases. BTPOA has been demonstrated to remain soluble in acid media even at high concentrations (≥5 M for 10 mM BTPOA solution).

Solubility is a key property in selecting the ligands for subsequent experiments. In addition to aqueous solubility, the maximum HNO_3 concentration at which each ligand remains soluble was considered, as the ligands are used in combination with an organic extractant. Under these conditions, TODGA is ineffective at relatively low HNO_3 concentrations. Consequently, BTPOA is the only suitable water-soluble ligand for solvent extraction and further investigations.

https://doi.org/10.1021/acs.iecr.5c04766
Ind. Eng. Chem. Res. 2026, 65, 6127−6142

Acid Constant Determination

The BTPOA pK_a value was determined through potentiometric titration and validated through the *Hyperquad* software. The potentiometric titration was performed with NaOH and HNO_3 measuring only a single equivalent point across all trials. The outcome differed from the expected range of eight points, suggesting the possibility of overlapping or undetectable equivalence points. To ascertain the single equivalence point, we employed the first derivative, calculating a value through the Henderson−Hasselbalch (eq 8), establishing an average pK_a value of 4.63 ± 0.05, with HA denoting the acid and A^- denoting the conjugate base of the ligand:

$$-\log[H_3O^+] = -\log[K_a] + \log\frac{[A^-]}{[HA]} \quad (8)$$

To corroborate the obtained pK_a through *Hyperquad*, we performed a titration with controlled ionic strength, fitting the experimental data in the program. This yielded four pK_a values, all of which were similar to those previously calculated.

The calculated pK_a value corresponds to those of the carboxylic acid family (~5), which would be expected for BTPOA. However, it is necessary to consider that the ligand can also be protonated at the pyridine nitrogen of the central ring in addition to the eight carboxylic groups in the periphery. The lowest pH value that could be measured with the available equipment was 0.99, which is above the pK_a for the pyridine nitrogen of 0.5 calculated for SO_3-Ph-BTP.[50] Therefore, the results obtained correspond to the eight carboxylic acid groups, and it is likely that all deprotonation occurred simultaneously.

Solvent Extraction

Figure 2 illustrates the distribution ratios of Am(III), Cm(III), and Eu(III) measured as a function of the HNO_3 concentration. Distribution ratios between 0.01 and 100 exhibit an uncertainty of ±5%, while lower/higher values exhibit larger uncertainties. It has been demonstrated that an increase in the HNO_3 concentration is indicative of an increase in the distribution ratios of all metal ions. This tendency is expected given that at high nitrate concentrations, TODGA exhibits a stronger complexation. In the case of increasing the concentration of HNO_3 (up to 1 M), the separation factor ($SF_{Eu/Am}$) of Eu compared to that of Am decreased significantly.

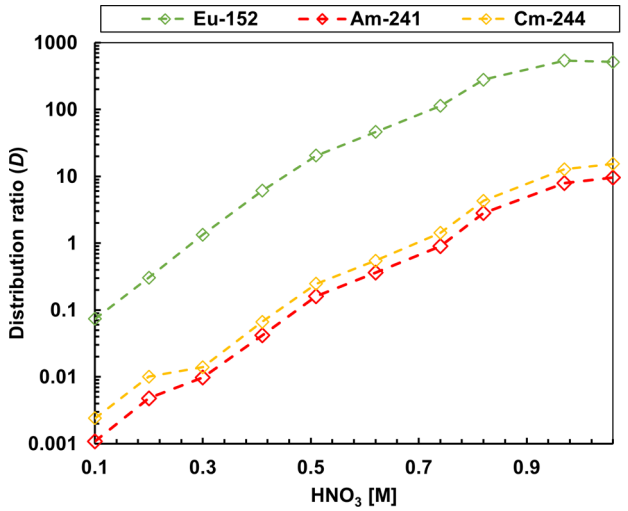

Figure 2. Distribution ratios as a function of the HNO_3 concentration. Exp. Cond.: Org: 0.2 M TODGA in 5 vol % octanol/TPH. Aq.: 0.01 M BTPOA in HNO_3 with 10 μM of each Ln(III) (w/o Pm), spiked with ^{241}Am(III), ^{244}Cm(III), and ^{152}Eu(III) at 22 °C and an O/A = 1.

Based on these data, the best concentrations for the performance of BTPOA and highest separation of An(III) and Ln(III) are 0.3−0.7 M HNO_3.

The next step was to compare the separation factors to determine whether the ligand can be a potential CHON candidate for the *i*-SANEX system as a replacement for SO_3-Ph-BTP. The separation factors are calculated as the quotient between the distribution ratios of two metals (*q.v.* SI-Methodology). Table 1 presents a comparison among the TODGA systems when used alone and in combination with either SO_3-Ph-BTP or BTPOA.

Table 1. Comparison of the Separation Factors in Different Systems[a]

SF	TODGA	TODGA/BTPOA	TODGA/SO_3-Ph-BTP[12]
$SF_{Eu(III)/Am(III)}$	~6	50−120	250−1000
$SF_{Cm(III)/Am(III)}$	~1.3	~1.5	~1

[a]Exp. cond.: separation factors are from 0.1 to 1 M HNO_3.

The combination of soft and hard donor atoms in BTPOA yields a synergistic effect,[17,51,52] which improves the resulting $SF_{Eu(III)/Am(III)}$. BTPOA achieves high separation factors between Ln(III) and An(III), with a considerable preference for An over Ln, in comparison with TODGA alone. However, the $SF_{Eu(III)/Am(III)}$ reached by SO_3-Ph-BTP was higher than that obtained with BTPOA. The octa-acid is nevertheless suitable as a replacement for SO_3-Ph-BTP in the *i*-SANEX system. The $SF_{Cm(III)/Am(III)}$ remains constant and unaltered by the concentration of HNO_3, with the SF corresponding mainly to the influence of TODGA. In this case, BTPOA shows a higher selectivity compared to that of SO_3-Ph-BTP.

We performed forward and backward extraction tests to observe the rate at which BTPOA forms complexes with the metal ions of interest. The difference between both tests relies on the number of steps involved. In the forward extraction, a single-step reaction, the organic phase contains the extractant, while the aqueous phase contains BTPOA, which has been dissolved in HNO_3 and mixed with the metal ions and radioactive tracers. In contrast, backward extraction comprises two steps. The first one involves loading the organic phase with the metals, Ln(III) and An(III), followed by the second step, which entails the An(III) being back-extracted into the aqueous phase with BTPOA. Figure 3 shows the distribution ratios of the selected metal ions at different extraction times.

The results indicated that BTPOA complexes with ^{241}Am, ^{244}Cm, and ^{152}Eu are formed in less than 5 min and remain stable over time, independent of the extraction direction.

The kinetic results for Ln(III) display different behavior between the light and heavy lanthanides. The light Ln(III)s exhibit fast kinetics for both extraction modes, which give consistent kinetic rate coefficient values. For the heavy Ln(III)s, there is a visible difference between forward and backward extraction modes, as shown in Figures 4 and 5, respectively. In the backward extraction, equilibrium is reached after 30 min, whereas in the forward extraction, equilibrium is attained after 50−60 min. This difference might be attributed to the size and charge density of the metal ions. Moreover, in

https://doi.org/10.1021/acs.iecr.5c04766
Ind. Eng. Chem. Res. 2026, 65, 6127−6142

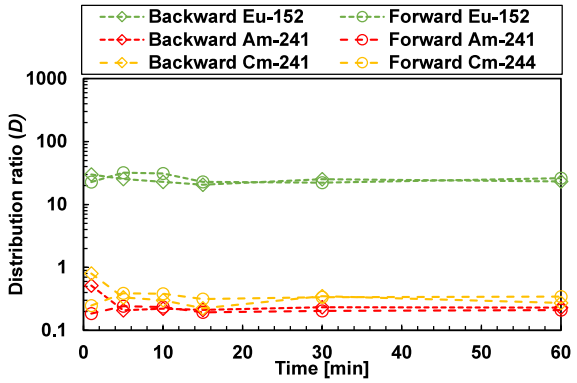

Figure 3. Forward and backward extractions as a function of time. Exp. cond.: Org.: 0.2 M TODGA in 5 vol % octanol/ISANE IP175. Aq.: 0.01 M BTPOA in 0.5 M HNO_3 with 10 μM Ln(III) (w/o Pm), spiked with ^{241}Am(III), ^{244}Cm(III), and ^{152}Eu(III) at 22 °C and an O/A = 1.

the context of forward extraction, a competitive dynamic exists between TODGA and BTPOA. Conversely, in the process of backward extraction, the extraction and back-extraction stages are executed by a single agent.

As an alternative hypothesis, the salting-in/out effect may be a contributing factor because the salting-out effect has been shown to increase the extraction rate and distribution ratios reflected in the backward extraction with the amount of NO_3^-.[53] The enhancement of extraction results has been demonstrated to increase the density of the aqueous phase. An alternative method that has been observed to yield a similar effect is the increase in the number of extractions, which consequently elevates the recovery rate.[54,55] In the case of BTPOA, a higher NO_3^- concentration inhibits the extraction of the metal ion into the organic phase.

The complexation of Am(III), Cm(III), and Eu(III) with BTPOA was studied as a function of the ligand concentration, as illustrated in Figure 6. This can be assessed using the slope analysis method, which is a graphical tool whose slope corresponds to the stoichiometric coefficients of the postulated chemical reaction for the ligand of interest. The bistriazinyl family obeys the following reaction (eq 9) for organic ligands:[14]

$$M_{aq}^{3+} + 3NO_3^- + 3L_{org} \rightleftharpoons M(L)_3(NO_3)_{3,org} \quad (9)$$

where M^{3+} corresponds to the metal ion, in our case An(III) or Ln(III), L denotes the organic ligand, NO_3^- corresponds to the nitrates present in the extraction, and the product of the reaction is the complex just formed.

However, the stoichiometry changes for water-soluble ligands have been postulated by Ruff et al.[56] for the reaction of water-soluble BTP during the back-extraction process. The first step is loading of the organic phase with the corresponding metals (eq 9). Afterward, the hydrophilic ligand complexes the metals, with the bistriazinyl group selectivity being higher for An(III) over Ln(III), the probability of occurrence for eq 10 is higher than that of eq 11:

$$[An(NO_3)_3(TODGA)_3)_{org}] + 3BTPOA \overset{K_{ex}}{\leftrightarrow} [An(BTPOA)_3]_{aq}^{x+} + 3NO_3^- + 3TODGA_{org} \quad (10)$$

$$[ln(NO_3)_3(TODGA)_3)_{org}] + 3BTPOA \overset{K_{ex}}{\leftrightarrow} [ln(BTPOA)_3]_{aq}^{x+} + 3NO_3^- + 3TODGA_{org} \quad (11)$$

where M^{3+} corresponds to the metal ion, in our case An(III) or Ln(III), L denotes the organic ligand, and $K_{ex,aq}$ is the extraction equilibrium constant. The $K_{ex,aq}$ is then defined as:

$$K_{ex,aq} = \frac{[An(BTPOA)]_{aq}^{x+} \times [NO_3^-]^3 \times [TODGA_{org}]^3}{[An(NO_3)_3(TODGA)_3)_{org}] \times [BTPOA]^{x+}} \quad (12)$$

The double-logarithmic graph of the distribution ratio and ligand concentration gives a linear equation, with the slope corresponding to the stoichiometric coefficients of the ligand. This enables calculation of the metal-to-ligand ratio. The slopes for Am(III), Cm(III), and Eu(III) were 1.34 ± 0.03, 1.32 ± 0.03, and 0.95 ± 0.06, respectively. These slopes differ significantly from an expected value of 3, as literature data suggests 1:3 complexes for BTP-type ligands.[14,56] Previous studies have reported inconsistent results in slope analysis for hydrophilic complexants with bistriazinyl−TODGA systems with slopes one order less than the real ratio.[14] However, in this case, the slope analysis resulted in two units less than the expected number.[14,18,56] Therefore, it was deemed necessary to determine the correct metal/ligand ratio with another technique. Thus, TRLFS measurements were performed to further elucidate this chemistry (see later).

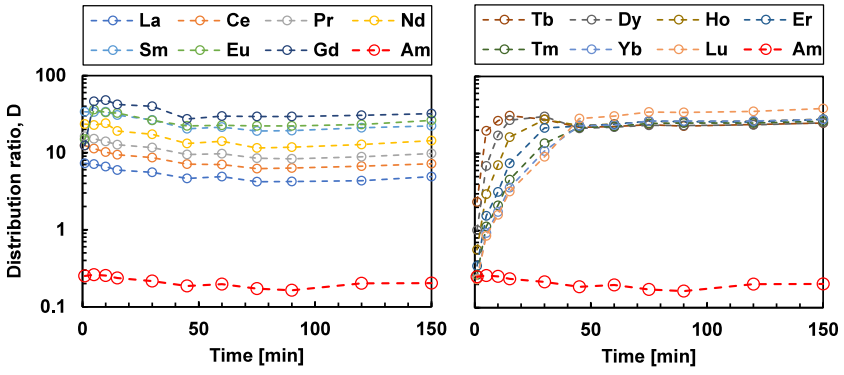

Figure 4. Forward extraction of the lanthanide series compared with Am(III). (Left: light Ln, right: heavy Ln) as a function of time. Exp. cond.: Org: 0.2 M TODGA in 5 vol % octanol/ISANE IP175. Aq.: 0.01 M BTPOA in 0.5 M HNO_3 with 10 μM Ln(III) (w/o Pm), spiked with ^{241}Am(III), ^{244}Cm(III), and ^{152}Eu(III) at 22 °C and an O/A = 1.

https://doi.org/10.1021/acs.iecr.5c04766
Ind. Eng. Chem. Res. 2026, 65, 6127−6142

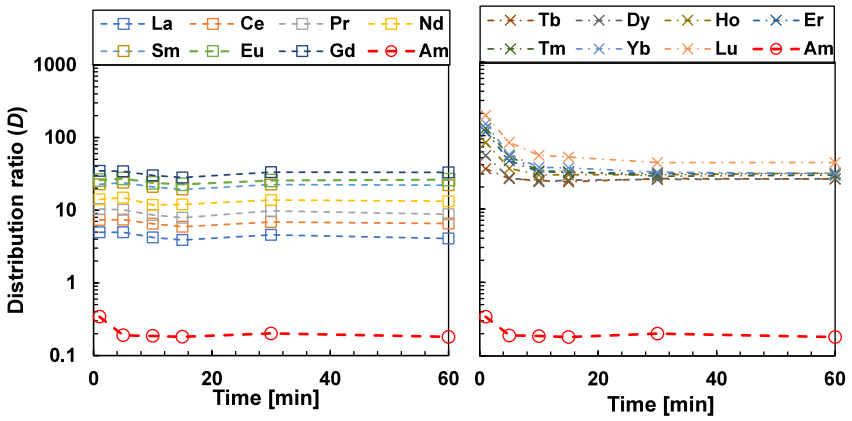

Figure 5. Backward extraction of the lanthanide series compared with that of Am(III). (Left: light Ln, right: heavy Ln) as a function of time. Exp. cond.: Org.: 0.2 M TODGA in 5 vol % octanol/ISANE IP175. Aq.: 0.01 M BTPOA in 0.5 M HNO_3 with 10 μM Ln(III) (w/o Pm), spiked with ^{241}Am(III), ^{244}Cm(III), and ^{152}Eu(III) at 22 °C and an O/A = 1.

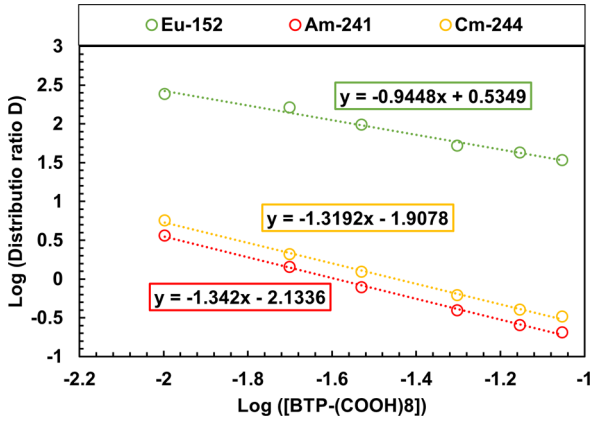

Figure 6. Am(III), Cm(III), and Eu(III) distribution ratios vs ligand concentration. Exp. cond: Org.: 0.2 M TODGA in 5 vol % octanol/TPH; Aq.: BTPOA acid in 0.82 M HNO_3 with 10 μM Ln(III) (w/o Pm), spiked with ^{241}Am(III), ^{244}Cm(III), and ^{152}Eu(III) at 22 °C and an O/A = 1.

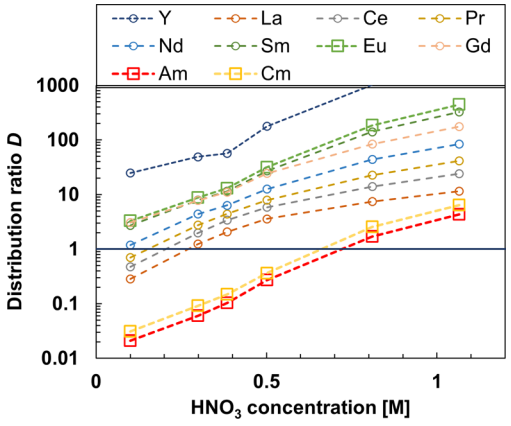

Figure 7. Experimental results of demonstration of the *i*-SANEX system. Exp. cond.: Org.: 0.2 M TODGA in 5 vol % octanol/ISANE IP175. Aq.: step 1:2.96 M HNO_3 HAR (Ln(III) and metals, see Table S1), step 2:0.5 M HNO_3 and spiked with ^{241}Am(III), ^{244}Cm(III), and ^{152}Eu(III). Step 3:0.01 M BTPOA in HNO_3 at 22 °C and an O/A = 1.

To observe the possible coextraction of An(III) or Ln(III) with other transition metals present in UNF and PUREX raffinates, BTPOA was tested over simulated high active raffinate (HAR), which contains light Ln(III) and other fission products (Ru, Rb, Sr, Zr, Mo, etc., see SI). During the loading of the organic phase, most of the non-Ln(III) fission products remained in the aqueous phase, and only Sr was extracted together with the light Ln(III). In the scrubbing step, ^{241}Am-(III), ^{152}Eu(III), and ^{244}Cm(III) were added and extracted into the organic phase, while most of the Sr(II) was back-extracted into the aqueous phase, leaving the loaded TODGA phase with minimal amounts of the non-Ln(III) fission products. In the stripping step, light Ln(III) and Y(III) remained in the organic phase, and Am(III) and Cm(III) were selectively back-extracted into the aqueous phase.

Figure 7 presents the distribution ratios of Ln(III), Am(III), and Cm(III) as a function of the HNO_3 concentration in the stripping step. Metal ion distribution ratios increased with increasing HNO_3 concentration, comparable to Figure 2. Due to the partial loading of TODGA, generally lower distribution ratios were observed, and La(III), Ce(III), and Pr(III) distribution ratios were <1 at the lowest tested HNO_3 concentration. Still, good selectivity between An(III) and all Ln(III)s was achieved, and between 0.3 and 0.5 M HNO_3 with high separation factors (e.g., $SF_{La/Am}$= 16 at 0.5 M), a selective separation of An(III) seems possible.

The extraction process was also tested at different temperatures. Figure 8 shows Am(III), Cm(III), and Eu(III) distribution ratios as a function of the temperature. The

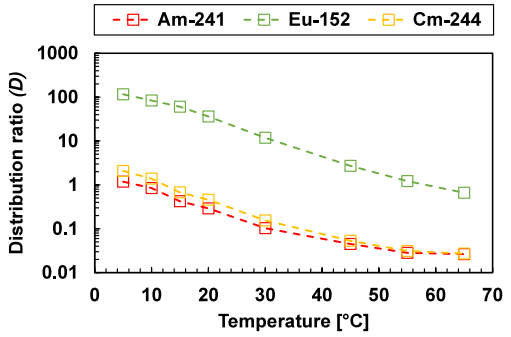

Figure 8. Distribution ratios of Am(III), Cm(III), and Eu(III) at 0.5 M HNO_3 as a function of the temperature (°C). Exp. cond.: Org.: 0.2 M TODGA in 5 vol % octanol/ISANE IP175. Aq.: 0.01 M BTPOA in 0.5 M HNO_3 with 10 μM Ln(III) (w/o Pm), spiked with ^{241}Am(III), ^{244}Cm(III), and ^{152}Eu(III) at an O/A = 1. Time: 30 min.

https://doi.org/10.1021/acs.iecr.5c04766
Ind. Eng. Chem. Res. 2026, 65, 6127−6142

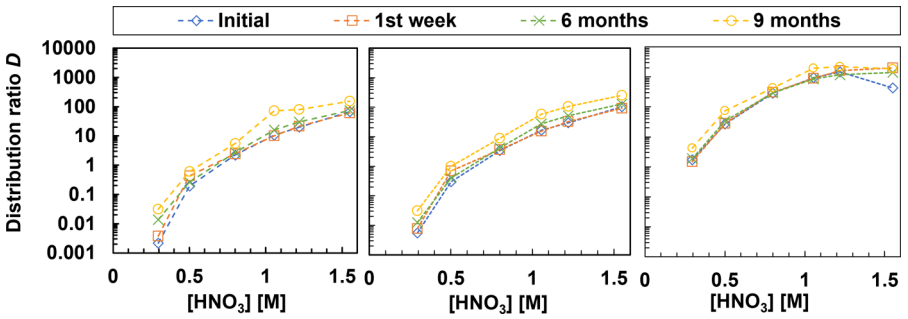

Figure 9. Hydrolysis experiment as a function of HNO_3 concentration over a 9-month period for $^{241}Am(III)$ (left), $^{244}Cm(III)$ (middle), and $^{152}Eu(III)$ (right). Exp. cond.: Org.: 0.2 M TODGA in 5 vol % octanol/ISANE IP175. Aq.: 0.01 M BTPOA in HNO_3 with 10 μM Ln(III) (w/o Pm) at 22 °C and an O/A = 1.

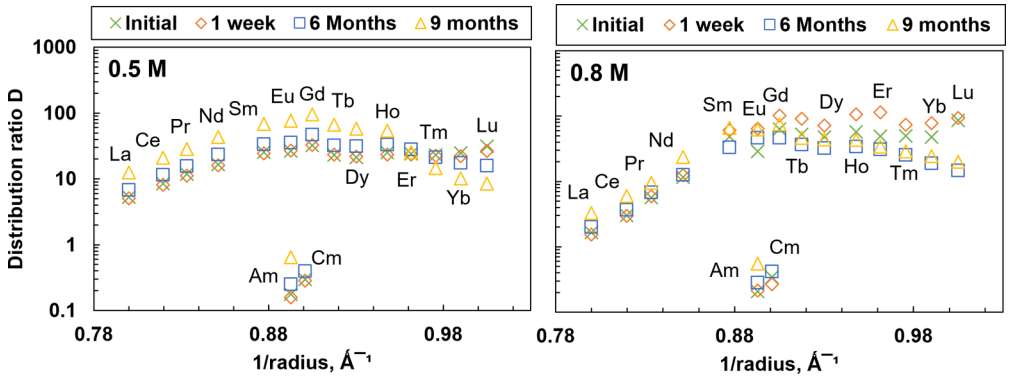

Figure 10. Hydrolysis experiment as a function of 1/radius over a 9-month period for Ln(III) at 0.5 and 0.8 M HNO_3. Exp. cond.: Org.: 0.2 M TODGA in 5 vol % octanol/ISANE IP175. Aq.: 0.01 M BTPOA in HNO_3 with 10 μM Ln(III) (w/o Pm) at 22 °C and an O/A = 1.

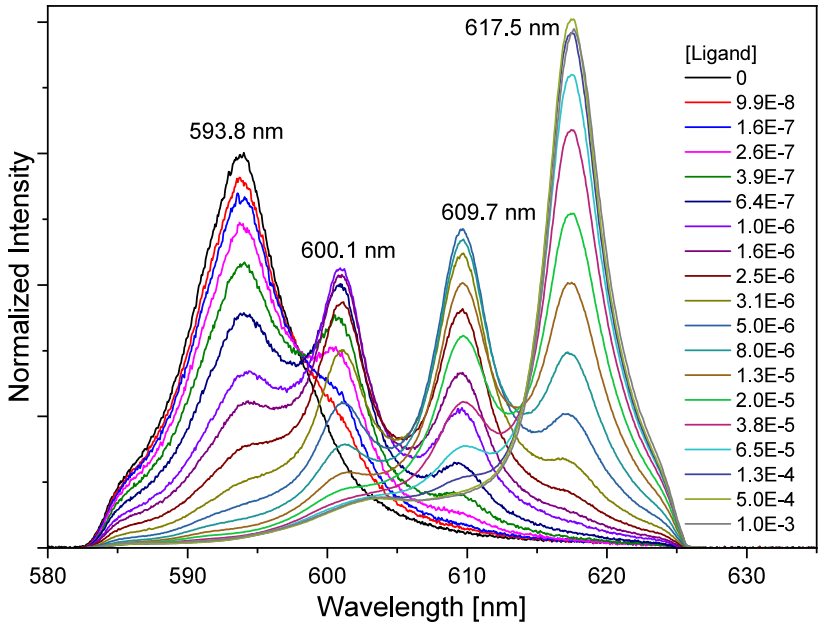

Figure 11. Normalized fluorescence spectra in 1 mM $HClO_4$ for the complexation of Cm(III) with BTPOA as a function of BTPOA concentration (0−1 mM).

distribution ratios decreased with increasing temperature, indicating that the system is exothermic, which is also observed in the TODGA system.

For solvent extraction thermodynamics studies, the exact stoichiometry and interaction of all ions and molecules involved in the reaction needs to be known, which is difficult to determine with two ligands in different phases. In this case, the TODGA stoichiometry is assumed to be 1:3,[57] with three additional NO_3^- involved in the complexation.[15] For BTPOA, a 1:3 species is currently assumed (see TRLFS section), but the amount of NO_3^- or water molecules is not confirmed. Therefore, further calculations, such as complexation data at

https://doi.org/10.1021/acs.iecr.5c04766
Ind. Eng. Chem. Res. 2026, 65, 6127−6142

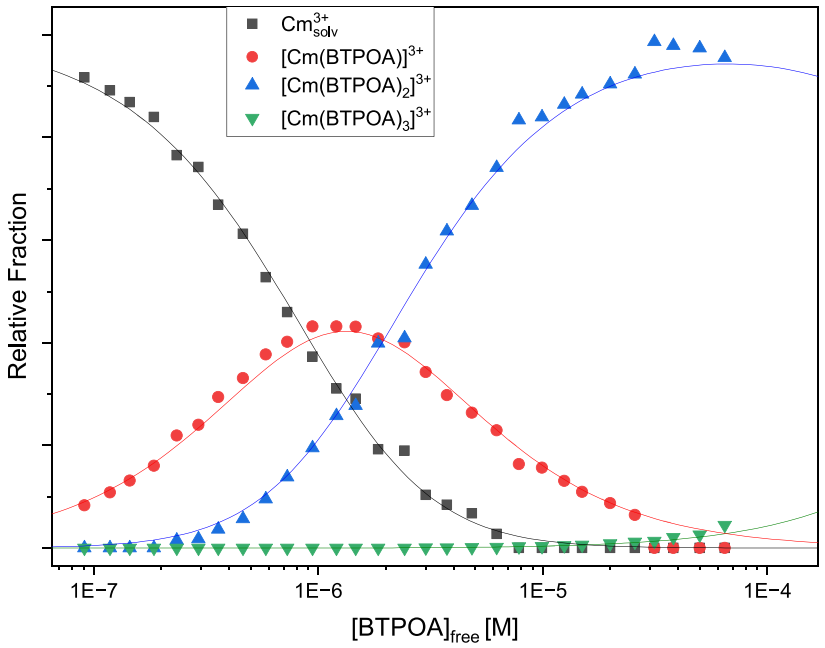

Figure 12. Speciation of Cm(III) as a function of noncomplexed BTPOA concentration in 1 mM $HClO_4$ with its corresponding trend lines.

different temperatures with each ligand and in combination with the available data, cannot be done.

As many of the hydrometallurgical processes for UNF management are carried out in HNO_3, it is crucial to obtain long-term knowledge of the stability of the ligand in acidic media. Hence, BTPOA was dissolved in different concentrations of HNO_3, and the solution was used in extraction experiments over a period of nine months.

Figure 9 shows the distribution ratios of ^{241}Am(III), ^{244}Cm(III), and ^{152}Eu(III), which present minimal changes after the first week. Six months later, the distribution ratios remained almost the same. The slight variations might be attributed to other factors, not particularly to the degradation of the ligand. After nine months, the distribution ratios started to increase slightly, showing the slow degradation of BTPOA.

The Ln(III) showed similar results at low HNO_3 concentrations, where the distribution ratios remain unchanged with time. However, as the concentration of HNO_3 increased, the values changed.

In Figure 10, we can observe the influence of HNO_3 concentration and the difference between light and heavy Ln(III)s, exhibiting, on average, a factor of 40 variation in their distribution ratios. The light Ln(III)s follow the expected trend, where the distribution ratios increased with time, whereas for heavy Ln(III)s, the distribution ratios decreased over time as the concentration of HNO_3 increased. This outcome needs to be further investigated. Overall, BTPOA is stable in 0.1−0.8 M HNO_3 solution for at least six months.

Speciation Studies Using TRLFS

In the same way that solvent extraction is fundamental to the characterization and assessment of BTPOA, TRLFS can be used to evaluate and complement the complexation data. The complexation of Cm(III) and Eu(III) was studied in two acid systems ($HClO_4$ and HNO_3) with a stock solution of 10 μM for Cm(III) and Eu(III). $HClO_4$ comprises a nonbinding anion, and only water and ligand molecules are expected to bind to the metal ion throughout the titration. In contrast, NO_3^- is a stronger ligand than ClO_4^- and can form weak complexes with metal ions.

Figure 11 shows the progression of the Cm(III) fluorescence spectra from the $^6D'_{7/2}$ to $\rightarrow{}^8S'_{7/2}$ transition with increasing ligand concentration. The Cm(III) aquo ion shows a single emission band at 593.8 nm.[58] With increasing ligand concentration, three emission bands with maxima at 600.1, 609.7, and 617.5 nm occur, corresponding to metal/ligand ratios of 1:1, 1:2, and 1:3, respectively. The bathochromic shifts (6, 16, and 24 nm) indicate a metal ion complexation by three nitrogen atoms of the ligands, and the addition of one ligand molecule per complexation step.[17]

The Cm(III) species distribution is derived by peak deconvolution of the fluorescence spectra using the single-component spectra given in Figure S7. To determine species concentrations, the fluorescence intensity factors (FI factors) of the different species must be considered. The FI factor of a complex species (FI_i) is calculated from the intensity ratio of species I_i and a reference species I_{ref} (eq 13). The solvent complex represents the reference species, whose FI factor FI_{ref} = 1:

$$FI_i = \frac{I_i}{I_{ref}} \tag{13}$$

The relative FI factor for the 1:3 complex is 180, while for the other two species it is 1. Figure 12 shows the species distribution as a function of the noncomplexed BTPOA concentration.

The noncomplexed ligand concentration was calculated according to eq 14:

$$[L]_{free} = 0.5 \times ((4 \times [L]_0 \times K_a + [H^+]_0^2 + 2 \times [H^+]_0 \times K_a + K_a^2)^{0.5} - [H^+]_0 - K_a) - ([Cm(III)] \times (\chi_{1:1} + 2 \times \chi_{1:2} + 3 \times \chi_{1:3})) \tag{14}$$

The complexation of BTPOA is described by eq 15 and the stoichiometry of the complex species can be determined by

https://doi.org/10.1021/acs.iecr.5c04766
Ind. Eng. Chem. Res. 2026, 65, 6127−6142

slope analyses (see Methods section) using the linear correlation between the logarithm of the noncomplexed ligand concentration and the concentration ratio between the species formed (eq 17). The slope analyses for the stepwise formation of the 1:1, 1:2, and 1:3 complex yielding slopes of 1 are shown in Figure S8. The conditional stability constants were calculated by the law of mass action (eqs 16 and 17). For the 1:1 complex $\log\beta'_1 = 6.06 \pm 0.05$, for the 1:2 complex $\log\beta'_2 = 11.75 \pm 0.11$, and for the final 1:3 complexation step, $\log\beta'_3 = 16.6 \pm 0.1$ was determined:

$$M[(solv)_9] + nL \rightleftharpoons ML_n (n = 1, 2, 3) \quad (15)$$

$$K_n = \frac{[ML_n]}{[M(solv)_9] \times [L]^n} \quad (16)$$

$$\log\left(\frac{[ML_n]}{[M(solv)_9]}\right) = \log K + n\log[L] \quad (17)$$

In comparison with SO_3-Ph-BTP,[59] the conditional stability constants of BTPOA complexes are larger, implying that it is a stronger binding ligand (Table 2). However, its extraction performance is worse under comparable chemical conditions, possibly due to the high number of carboxylic acid groups, as the deprotonated carboxylic acid groups could also complex the metal ions in addition to the nitrogen atoms from the pyridine and triazine rings, which hinders the extraction process, since the metal is not located in the right coordination site, giving place to faster dissociation or lowering the coordination constants.

Table 2. Comparison of Conditional Stability Constants of SO_3-Ph-BTP and BTPOA in $HClO_4$

stability constant	SO_3-Ph-BTP[59a]	BTPOA
$\log \beta'_1$	5.4 ± 0.1	6.0 ± 0.2
$\log \beta'_2$	9.3 ± 0.2	11.8 ± 0.2
$\log \beta'_3$	12.2 ± 0.3	14.4 ± 0.2

[a] SO_3-Ph-BTP exp. cond. $[Cm(ClO_4)_3]^{3+}$ 0.12 μM, pH 3.0 with 1 mM $HClO_4$. Equilibrium time: 15 min.

Figure 13 shows the emission spectra of Cm(III) with BTPOA in the presence of 0.5 M HNO_3. The emission band at 594.2 nm is assigned to the Cm(III) aquo species ($[Cm(H_2O)_9]^{3+}$) and the emission band at 597.2 nm to the ($[Cm(H_2O)_9NO_3]^{2+}$) species, in agreement with Ruff et al.[56] With increasing BTPOA concentration, two emission bands at 609.5 and 617.8 nm occur. Evaluation of the emission band at 609.5 nm shows that two different 1:2 complexes are formed (Figure S10). The emission band at 617.8 nm corresponds to the 1:3 complex.

A plausible explanation for the existence of two 1:2 complexes displaying different spectroscopic shifts is the replacement of a water molecule in the inner coordination sphere by NO_3^-, as the difference in wavelength is too small to be assigned to a different complexation mode (O vs. N).

Since the ligand presents a high FI factor of (116) for the 1:3 species, this FI factor must be considered to determine species concentrations. The species distribution, including the two different 1:2 complex species, is shown in Figure 14.

Table 3 shows a comparison of the conditional stability constants of the Cm 1:3 complexes with BTPOA and SO_3-Ph-BTP in the $HClO_4$ and HNO_3 systems. In the presence of NO_3^-, the stability constant of the 1:3 complex decreases by several orders of magnitude. This is in line with the stronger complexation properties of NO_3^- compared to ClO_4^-. However, in the NO_3^- medium, the stability constants of the 1:3 complexes of Cm(III) with BTPOA and SO_3-Ph-BTP are comparable.

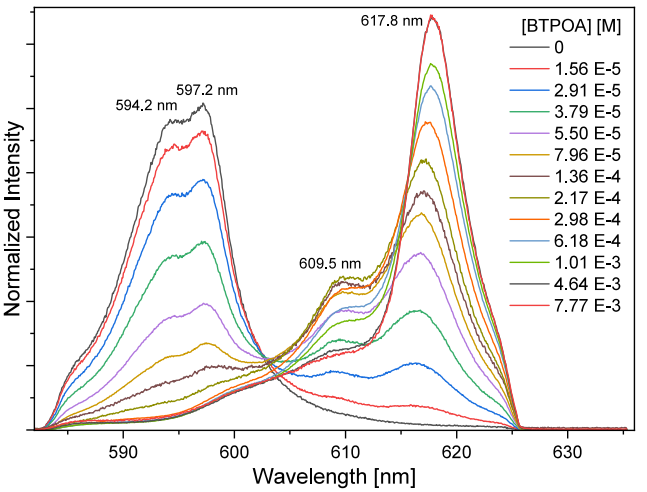

Figure 13. Normalized fluorescence emission spectra in 0.5 M HNO_3 for the complexation of Cm(III) with BTPOA as a function of the BTPOA concentration (0−7.77 mM).

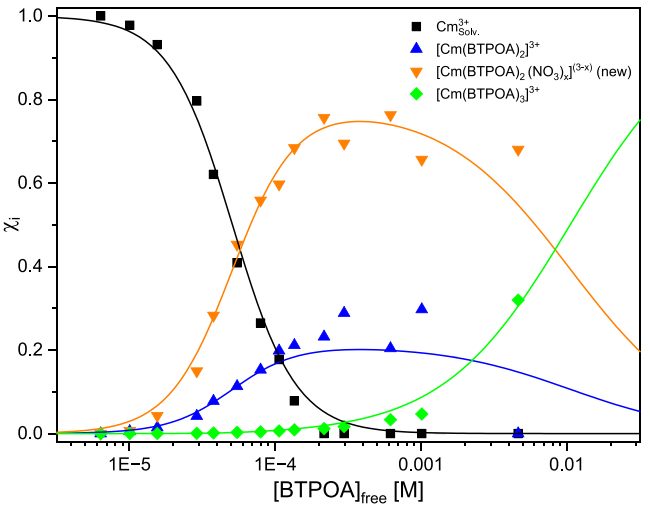

Figure 14. Speciation of Cm(III) as a function of the concentration of BTPOA in 0.5 M HNO_3 with its corresponding trend lines.

Table 3. Comparison of the Conditional Stability Constants of Cm(III) of 1:3 Complexes with BTPOA and SO_3-Ph-BTP[59] in $HClO_4$ and HNO_3

	0.5 M HNO_3		1 mM $HClO_4$	
$\log \beta'_n$	BTPOA	SO_3-Ph-BTP	BTPOA	SO_3-Ph-BTP[59]
3	10.6 ± 0.4	10.6	14.4 ± 0.4	12.2

Additionally, the organic and aqueous phases were measured in TRLFS. These were produced from the extraction using the same conditions as for the solvent extraction experiments. This was done in order to identify which species are formed during extraction.

Figure 15 shows the emission spectrum of Cm(III) in the aqueous phase after extraction and the $[Cm(BTPOA)_3]^{x+}$

https://doi.org/10.1021/acs.iecr.5c04766
Ind. Eng. Chem. Res. 2026, 65, 6127−6142

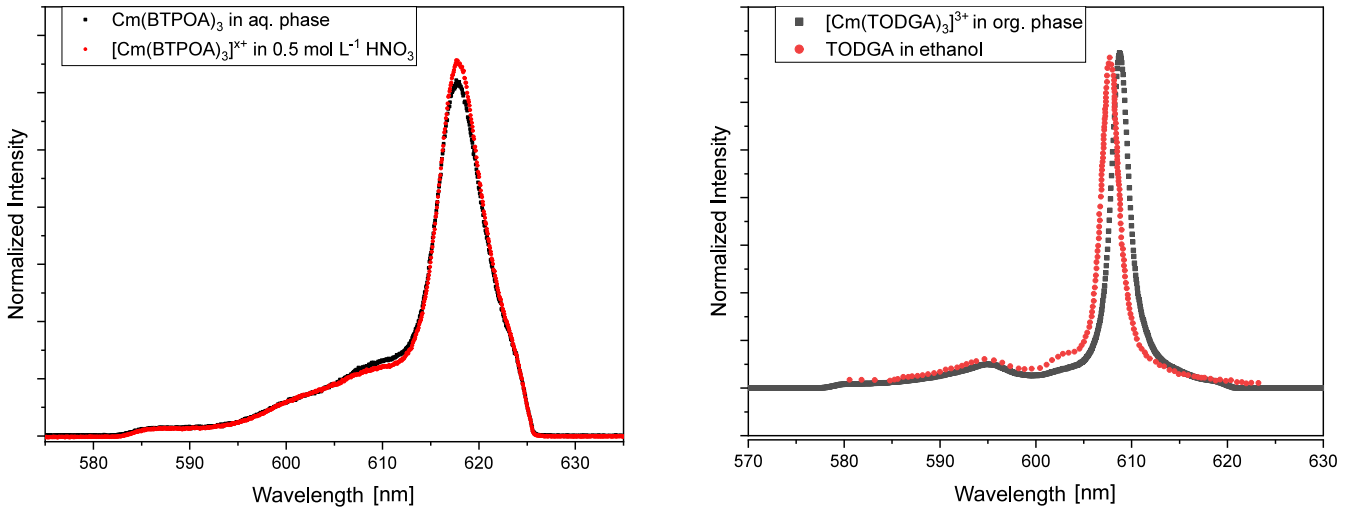

Figure 15. Left: Normalized Cm(III) spectrum in the aqueous phase after extraction and emission spectrum of $[Cm(BTPOA)_3]^{x+}$. Right: Normalized Cm(III) spectrum in the organic phase after extraction and spectrum of the 1:3 TODGA complex in ethanol.[60] Exp. cond: organic phase: 0.2 M TODGA in 5 vol % octanol/TPH. Aqueous phase: 10 mM BTPOA spiked with 10 μM Cm(III).

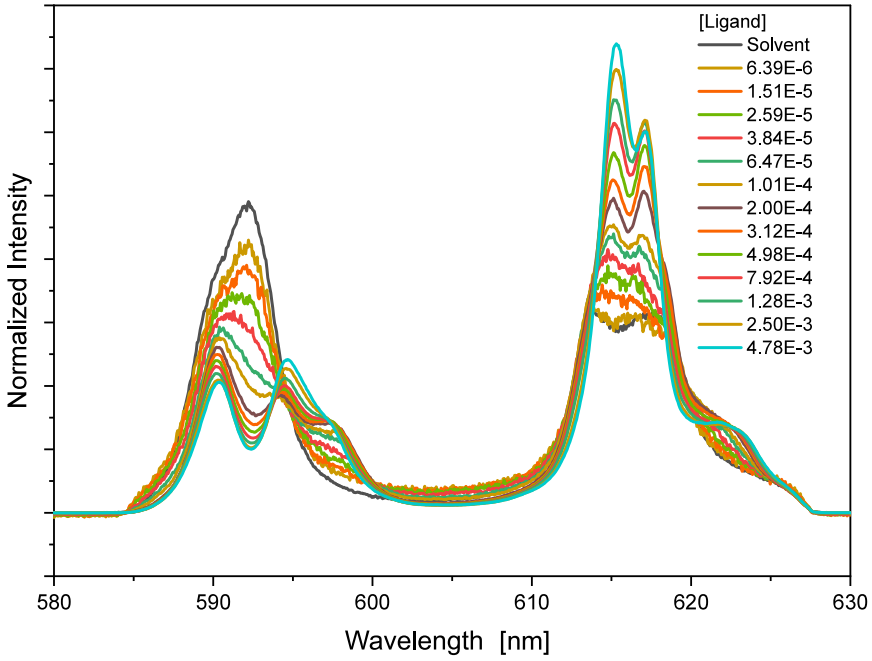

Figure 16. Normalized emission spectra for the complexation of Eu(III) ($^7F_1$ and $^7F_2$ bands) with BTPOA in 0.5 M HNO_3 as a function of the BTPOA concentration.

complex in HNO_3 (left). Both spectra are identical, which confirms the formation of 1:3 Cm(III)-BTPOA under extraction conditions. In the organic phase (right), the spectrum after extraction agrees with the one of the 1:3 Cm(III) complexes with TODGA in ethanol.[61] The small deviation in the peak position is caused by the different organic solvents used (TPH and IP175). Thus, it was possible to identify the extraction-relevant Cm(III) complex species by a comparison with the results of monophasic speciation studies.

To study the differences in the complexation properties of BTPOA toward An(III) and Ln(III), further speciation studies were performed with Eu(III). Due to the very high FI factors of the complexed species, quantitative speciation studies of Eu(III) with BTPOA in $HClO_4$ were not possible. However, the FIs were found to be lower in HNO_3, allowing the titration to be conducted over a wider range of ligand concentrations and the deconvolution of the emission spectra. The normalized emission spectra of Eu(III) with BTPOA resulting from the $^5D_0 \rightarrow {}^7F_1$ and $^5D_0 \rightarrow {}^7F_2$ transitions are shown in Figure 16.

In the absence of BTPOA, the solvent spectrum of Eu(III) is characterized by two emission bands at 592 nm ($^7F_1$ band) and 612.2 nm/615.6 nm ($^7F_2$ band). Upon the addition of the ligand, the relative intensity of the $^7F_1$ band decreases, while two new peaks evolved at 590.45 and 594.51 nm. Regarding the $^7F_2$ band, two sharp peaks at 615.73 and 617.27 nm are observed with progressive complexation. Deconvolution of the emission spectra showed the formation of three different complex species: $[Eu(BTPOA)_n]^{x+}$ (n = 1, 2, or 3). Again, the FI factor (180) of the 1:3 complex is much higher than those for the other two species, which must be considered when

https://doi.org/10.1021/acs.iecr.5c04766
Ind. Eng. Chem. Res. 2026, 65, 6127−6142

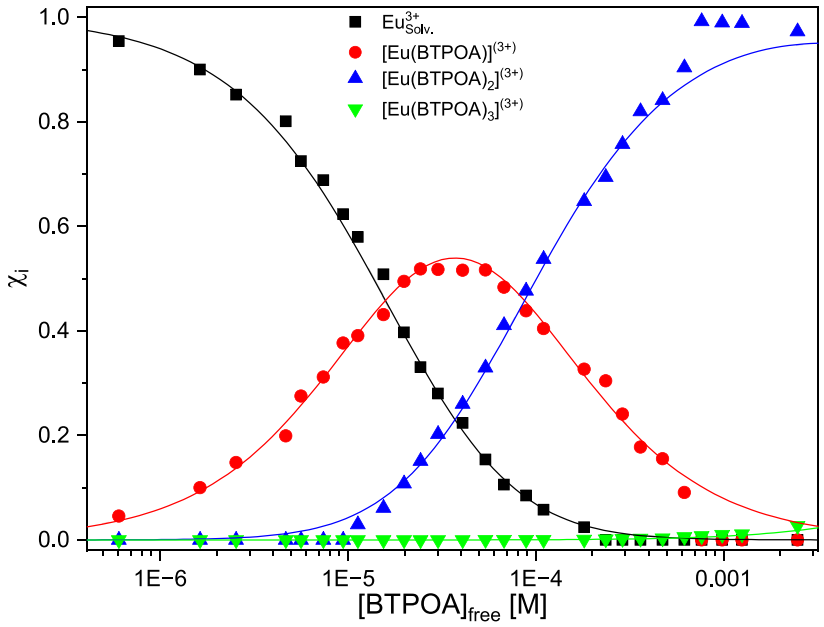

Figure 17. Speciation of Eu(III) as a function of the concentration of noncomplexed BTPOA in 0.5 M HNO_3 with its corresponding trend lines.

Table 4. Summary of Measured Second-Order Rate Coefficients for the Reaction of BTPOA with Aqueous Phase Transient Radiolysis Products in Comparison to Values for Its Sulfonated Analogue, SO_3-Ph-BTP

	second-order rate coefficient (k, M^{-1} s^{-1})			
ligand	e_{aq}^- ($\times 10^{10}$)	$H^\bullet$ ($\times 10^9$)	$^\bullet OH$ ($\times 10^9$)	$NO_3^\bullet$ ($\times 10^7$)
SO_3-Ph-BTP[39]	1.51 ± 0.01	3.07 ± 0.11	2.38 ± 0.14	3.72 ± 0.13
BTPOA	1.60 ± 0.02	2.17 ± 0.03	6.95 ± 0.06	0.37 ± 0.02

calculating the species concentrations. The species distribution is shown in Figure 17.

The stoichiometry of the different Eu(III) BTPOA complexes is confirmed by slope analyses according to a stepwise complexation model. Plotting the logarithm of ($[Eu(BTPOA)_n]^{x+}/Eu(BTPOA)_{n-1}]^{x+}$) as a function of the logarithm of the noncomplexed BTPOA concentration (see Figure S11) results in slopes of 1 for each complex species (n = 1, 2, or 3).

Based on the resolved speciation, the corresponding conditional stability constants were calculated: $\log\beta_1 = 4.9 \pm 0.2$, $\log\beta_2 = 8.9 \pm 0.3$, and $\log\beta_3 = 9.8 \pm 0.4$. The stability constants of the extraction-relevant 1:3 complexes for Cm(III) and Eu(III) in HNO_3 differ by 0.8 orders of magnitude, confirming a weaker binding of Ln(III) compared to that of An(III). This trend is consistent with and corroborated by the solvent extraction experiments.

Radiation-Induced BTPOA Reaction Kinetics

Another key property in the evaluation of potential UNF extractants is their behavior in ionizing radiation fields, as this dictates their viability under the envisioned process conditions. In this regard, radical reaction kinetics provide valuable mechanistic insights that can be leveraged to support computational predictions on a ligand's radiolytic longevity. The reaction kinetics for this study were measured using the Notre Dame Radiation Research Laboratory (NDRL) pico-to-nanosecond electron-pulsed linear accelerator (LINAC) and transient absorption detection system.[62,63] The results are summarized in Table 4, along with previously derived values for SO_3-Ph-BTP.

Concerning the chemically reducing radiolysis products (e_{aq}^- and $H^\bullet$), the substitution of sulfophenyl groups (SO_3-Ph-BTP) for octa acid functionalities (BTPOA) was found to have a negligible impact on the ligand's reactivity (Table 4, SI Figures S12 and S13, respectively). This observation indicates that reduction does not take place at the hydrophilic functional groups (R−SO_4H nor R−CO_2H), but instead with the BTP core structure. Given similar measurements for the reaction of the e_{aq}^- with aromatic pyridine ($k = 3.7 \times 10^9$ M^{-1} s^{-1})[64] and triazine ($k = 5.2 \times 10^9$ M^{-1} s^{-1})[65] containing molecules, we can assume that the electron reaction occurs at both these moieties within BTPOA. For the $H^\bullet$ reaction, the much slower rate coefficients for its reaction with pyridine ($k = 2.2 \times 10^8$ M^{-1} s^{-1})[66] suggests that the majority of $H^\bullet$-reactivity occurs with the triazine moiety in this molecule (no specific triazine literature rate coefficient could be found).

Although these new reducing radical reaction rate coefficients were measured under optimal solution conditions, such as at neutral pH for e_{aq}^-, they are still important for the development of comprehensive predictive models for the radiation-induced behavior of BTPOA. Based on these kinetic data, it can readily be seen that under envisioned process conditions—aerated, aqueous HNO_3 solution—these reducing transient species are rapidly scavenged by NO_3^- (eqs 4 and 5), acidic protons (H_{aq}^+, eq 18), and dissolved O_2 (eqs 19 and 20):[40]

$$e_{aq}^- + H_{aq}^+ \rightarrow H^\bullet \quad k_{17} = 2.3 \times 10^{10}\ M^{-1}s^{-1} \tag{18}$$

$$e_{aq}^- + O_2 \rightarrow O_2^{\bullet-} \quad k_{18} = 1.9 \times 10^{10}\ M^{-1}s^{-1} \tag{19}$$

https://doi.org/10.1021/acs.iecr.5c04766
Ind. Eng. Chem. Res. 2026, 65, 6127−6142

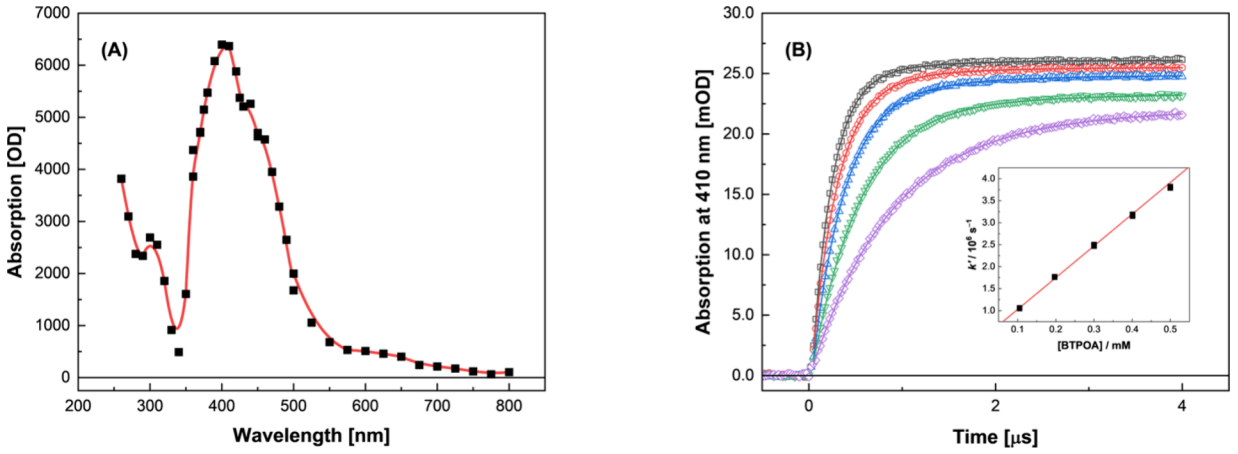

Figure 18. (A) Transient absorption spectra arising from the electron pulse irradiation of 500 μM BTPOA in N_2O-saturated 10 mM phosphate buffer solution at pH 7.0 ± 0.1 and 24.6 °C. (B) Corresponding pseudo-first-order transient growth kinetics observed at 410 nm for 105 (purple), 197 (green), 300 (blue), 401 (red), and 500 (gray) μM BTPOA. *Inset:* Second-order rate coefficient determination using the fitted pseudo-first-order component values: (1.09 ± 0.01) × 10^6, (1.85 ± 0.01) × 10^6, (2.63 ± 0.01) × 10^6, (3.37 ± 0.02) × 10^6, and (4.20 ± 0.03) × 10^6 s^{-1}, respectively. The solid line is a weighted linear fit to transformed data, corresponding to k(BTPOA + •OH) = (6.95 ± 0.06) × 10^9 M^{-1} s^{-1}, R^2 = 0.998.

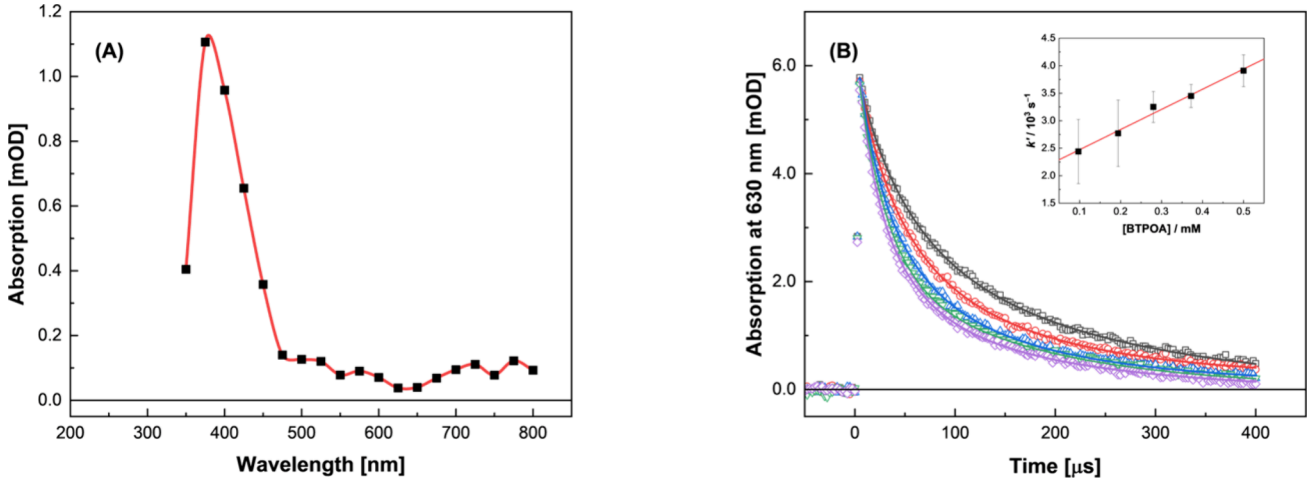

Figure 19. (A) Transient absorption spectra arising from the electron pulse irradiation of 500 μM BTPOA in a 6.0 M HNO_3 solution at 24.5 °C. (B) Corresponding double first-order transient decay kinetics observed at 630 nm for 97.1 (gray), 194 (red), 280 (blue), 372 (green), and 500 (purple) μM BTPOA. *Inset:* Second-order rate coefficient determination using the fitted pseudo first-order component values (1.53 ± 0.07) × 10^4, (1.97 ± 0.05) × 10^4, (2.26 ± 0.04) × 10^4, (2.77 ± 0.07) × 10^4, and (3.14 ± 0.08) × 10^4 s^{-1}, respectively. The solid line is a weighted linear fit to transformed data, corresponding to k(BTPOA + NO_3•) = (3.70 ± 0.20) × 10^6 M^{-1} s^{-1}, R^2 = 0.987.

$$H^\bullet + O_2 \rightarrow HO_2^\bullet \quad k_{19} = 1.2 \times 10^{10}\ M^{-1}s^{-1} \tag{20}$$

and thus, likely unavailable for reaction with BTPOA. Consequently, the radiolytic behavior of BTPOA is expected to be driven by the oxidizing products of aqueous HNO_3 radiolysis, specifically •OH and NO_3•.

Under dilute HNO_3 conditions, there is only a small amount of undissociated HNO_3 (eq 3), and thus, •OH will be competitively available for reaction with BTPOA. This reaction was found to give a strongly absorbing transient species, as shown in Figure 18A.

By monitoring the growth rate of this species' absorption at 410 nm (Figure 18B) and fitting these kinetics to an exponential growth equation:

$$k = \mathrm{Abs}^o(1 - e^{-k't}) + B \tag{21}$$

where Abs^o is the limiting transient absorbance, k' is the pseudo-first-order rate coefficient for •OH + BTPOA, t is time, and B is a baseline adjustment parameter, a plot of k' vs [BTPOA] then gives a straight line (see Figure 18B, *Inset*) whose slope corresponds to a second-order rate coefficient of k = (6.95 ± 0.06) × 10^9 M^{-1} s^{-1}. This value is more than twice as fast as that previously measured for the analogous SO_3-Ph-BTP molecule (Table 4), indicating that there is chemical reactivity between the •OH and the hydrophilic BTP functional groups, with the reaction at the carboxyl groups being more energetically favorable than at the sulfonate groups. The •OH typically removes a beta-hydrogen atom from carboxylic acid molecules;[40] however, BTPOA does not possess beta-hydrogen atoms adjacent to its hydrophilic functional groups. As such, we anticipate that the •OH will add to the aromatic rings adjacent to BTPOA's carboxyl groups, thereby forming the observed transient adduct, cyclohexadienyl-type, species. This is in keeping with the chemical interactions between the •OH and other aromatic compounds.[40] The greater susceptibility of BTPOA vs SO_3-Ph-

https://doi.org/10.1021/acs.iecr.5c04766
Ind. Eng. Chem. Res. 2026, 65, 6127−6142

BTP to the reaction with $^{\bullet}OH$ may be attributed to a combination of: (*i*) differences in the electron richness of the adjacent aromatic rings, due to the lower electron withdrawing capacity of R-COOH (Hammett constant, $s = -0.37$) vs R-SO_3H ($s = -0.51$);[67] and (*ii*) changes in steric hindrance, with the sulfonate groups being larger, thereby somewhat shielding the aromatic rings.

Under more concentrated HNO_3 conditions, the $^{\bullet}OH$ is completely replaced by $NO_3^{\bullet}$ (eq 6), which has also been shown to exhibit significant reactivity toward reprocessing ligands. As with $^{\bullet}OH$, the reaction between BTPOA and $NO_3^{\bullet}$ afforded an observable transient species, the absorption spectrum for which is given in Figure 19A. The spectrum of this species closely resembles that from the $^{\bullet}OH$ reaction (Figure 18A), suggesting a perturbation similar to that of the triazine/pyridine rings.

Concerning the reaction kinetics for this process, the decay of $NO_3^{\bullet}$ was directly monitored at 630 nm as a function of the concentration of BTPOA. The measured decays, shown in Figure 19B, were fit using two first-order decay functions:

$$\text{Abs} = A_1{}^{*}\exp(-k'_{\text{BTPOA}}t) + A_2{}^{*}\exp(-k't) + B \quad (22)$$

where Abs is the transient absorption intensity of $NO_3^{\bullet}$, k'_{BTPOA} and k' are the pseudo-first-order rate coefficients for the $NO_3^{\bullet}$ reaction with BTPOA and other aqueous HNO_3 radiolysis product species, respectively:[40]

$$NO_3^{\bullet} + OH^{\bullet} \rightarrow NO_2^{\bullet} + HO_2^{\bullet} \quad k = 1.0 \times 10^{10}\ M^{-1}s^{-1} \quad (23)$$

$$NO_3^{\bullet} + H_2O \rightarrow HNO_3 + OH^{\bullet} \quad k = 300\ M^{-1}s^{-1} \quad (24)$$

$$NO_3^{\bullet} + NO_2^{-} \rightarrow NO_3^{-} + NO_2^{\bullet} \quad k = 4.4 \times 10^{9}\ M^{-1}s^{-1} \quad (25)$$

$$NO_3^{\bullet} + NO_2^{\bullet} \rightarrow N_2O_5 \quad k = 1.1 \times 10^{9}\ M^{-1}s^{-1} \quad (26)$$

$$NO_3^{\bullet} + HNO_2 \rightarrow HNO_3 + NO_2^{\bullet} \quad k = 2.0 \times 10^{8}\ M^{-1}s^{-1} \quad (27)$$

A_1 and A_2 are the corresponding fractions of $NO_3^{\bullet}$ reacting by each pathway, and B accommodates for any limiting product absorption, i.e., a baseline shift. The k'_{BTPOA}-fitted values were then plotted against concentration (Figure 19B, *Inset*) to give the second-order rate coefficient, as shown in Table 4. Interestingly, the reaction of BTPOA with $NO_3^{\bullet}$ is an order of magnitude slower than that of the corresponding SO_3-Ph-BTP reaction. This difference is contrary to our previous $^{\bullet}OH$ findings.

Although gamma-dose accumulation studies were attempted—using the NDRL's Nordion Gammacell 220 and a Shepherd 109−68 cobalt-60 irradiators—characterization of the resulting samples was complicated by the BTPOA molecule's tendency to fragment during LC analysis. In lieu of such experimental results, the above measured reaction kinetics can be used to make some assumptions about the radiolytic longevity of BTPOA under envisioned process conditions. This is especially true given that previous calculations found that the gamma radiolysis of SO_3-Ph-BTP was predominantly driven (~90%) by its reaction with $^{\bullet}OH$ in aqueous solutions.[40] In the case of BTPOA, we anticipate this molecule to exhibit greater longevity in a gamma radiation field as compared to SO_3-Ph-BTP under the optimized process conditions outlined earlier: 0.3−0.7 M HNO_3. This is because $NO_3^{\bullet}$ will be the predominant oxidant, not $^{\bullet}OH$, which reacts an order of magnitude slower with BTPOA compared to SO_3-Ph-BTP (Table 4). This is a fortuitous finding for advancing flowsheet development for BTPOA-based separations technology.

CONCLUSIONS

BTPOA is a promising CHON alternative to SO_3-Ph-BTP for An/Ln separation in the *i*-SANEX system through solvent extraction. The results show the optimal HNO_3 concentration range is 0.3−0.7 M, reaching the highest separation factors ($SF_{Eu/Am} \sim 120$) in the TODGA system. However, BTPOA does not reach the same high values as its sulfonated analogue. The complexation reaction was fast, reaching equilibrium for An(III) and light Ln(III) in ca. 10 min. For heavy Ln(III), equilibrium is reached within a time frame of 30−50 min. A remarkable stability against hydrolysis was found in low HNO_3 concentrations (≤0.8 M) over a six-month period. At higher HNO_3 concentrations (≥0.8 M), the observed results indicate slight changes in metal ion complexation that could be related to acid-induced hydrolysis.

The slope analysis conducted with solvent extraction yielded inconclusive data, whereas the TRLFS method revealed the formation of 1:3 complexes for Cm(III) and Eu(III) during extraction. Conditional stability constants for Cm(III) in $HClO_4$ indicate that BTPOA is a stronger ligand than its analogue SO_3-Ph-BTP. However, in NO_3^{-} media, lower conditional stability constants were found, though these were similar to those identified for SO_3-Ph-BTP. The remarkably high FI factor exhibited by Eu(III) hindered the determination of conditional stability constants using TRLFS.

The BTPOA molecule was also found to react with all four common reprocessing radical products from aqueous phase radiolysis—the e_{aq}^{-}, $H^{\bullet}$, $^{\bullet}OH$, and $NO_3^{\bullet}$. Notably, substitution of R-SO_3H with R-COOH groups, in going from SO_3-Ph-BTP to BTPOA, resulted in a significant reduction (by an order of magnitude) in reactivity toward $NO_3^{\bullet}$. This finding is promising for the longevity and recyclability of a BTPOA-based separation solvent, as the rate of BTPOA radiolysis is expected to significantly decrease with increasing HNO_3 concentration, which corresponds with an increasing prevalence of $NO_3^{\bullet}$. However, additional studies are necessary to assess the effect of actinide complexation on the radiolytic longevity of BTPOA.[48]

ASSOCIATED CONTENT

Supporting Information

The Supporting Information is available free of charge at https://pubs.acs.org/doi/10.1021/acs.iecr.5c04766.

Experimental details, materials, and equipment for the experiments; additional graphs from solvent extraction experiments; pK_a determination; TRLFS titration; pulse radiolysis experiments; and reaction kinetics figures for the reaction of BTPOA with the e_{aq}^{-} and $H^{\bullet}$ (PDF)

AUTHOR INFORMATION

Corresponding Author

Andreas Wilden − *Forschungszentrum Jülich GmbH, Institute of Fusion Energy and Nuclear Waste Management−Nuclear Waste Management (IFN-2), Jülich 52428, Germany;*

https://doi.org/10.1021/acs.iecr.5c04766
Ind. Eng. Chem. Res. 2026, 65, 6127−6142

orcid.org/0000-0001-5681-3009; Email: a.wilden@fz-juelich.de

Authors

Laura Diaz Gomez − *Forschungszentrum Jülich GmbH, Institute of Fusion Energy and Nuclear Waste Management−Nuclear Waste Management (IFN-2), Jülich 52428, Germany*

Patrik Weßling − *Heidelberg University, Institute of Physical Chemistry, Heidelberg 69120, Germany*

Petra J. Panak − *Heidelberg University, Institute of Physical Chemistry, Heidelberg 69120, Germany*

Gregory P. Horne − *Center for Radiation Chemistry Research, Idaho National Laboratory, Idaho Falls ID83415, United States;* orcid.org/0000-0003-0596-0660

Stephen P. Mezyk − *Department of Chemistry and Biochemistry, California State University Long Beach, Long Beach, California 90840-9507, United States*

Julie R. Peller − *Department of Chemistry, Valparaiso University, Valparaiso, Indiana 46383, United States*

Andreas Geist − *Karlsruhe Institute of Technology (KIT), Institute for Nuclear Waste Disposal (INE), Karlsruhe 76021, Germany*

Giuseppe Modolo − *Forschungszentrum Jülich GmbH, Institute of Fusion Energy and Nuclear Waste Management−Nuclear Waste Management (IFN-2), Jülich 52428, Germany*

Complete contact information is available at: https://pubs.acs.org/10.1021/acs.iecr.5c04766

Notes

The authors declare no competing financial interest.

■ ACKNOWLEDGMENTS

This research was funded by the SEPAM (02 E 11921A) Project sponsored by the Federal Ministry of Environment, Nature Conservation, Nuclear Safety and Consumer Protection. G.P.H. was supported by the U.S. Department of Energy (US-DOE), Office of Science (SC), Office of Basic Energy Sciences (BES), Photochemistry and Radiation Chemistry Program under award DE-SC0024191. S.P.M. and J.R.P. were supported by the US-DOE and the Assistant Secretary for Nuclear Energy, under the Material Recovery and Waste Form Development Campaign, DOE-Idaho Operations Office Contract DE-AC07-05ID14517. Irradiations performed at the NDRL were supported by the Division of Chemical Sciences, Geosciences and Biosciences, Basic Energy Sciences, Office of Science, US-DOE through Award No. DE-FC02-04ER15533.

■ REFERENCES

(1) Lanham, W. B.; Runion, T. C. *PUREX Process for Plutonium and Uranium Recovery*; ORNL-479; Oak Ridge National Laboratory: Oak Ridge, TN, USA, 1949.

(2) Kooyman, T. Current state of partitioning and transmutation studies for advanced nuclear fuel cycles. *Ann. Nucl. Energy* **2021**, *157*, No. 108239.

(3) OECD-NEA. *Potential Benefits and Impacts of Advanced Nuclear Fuel Cycles with Actinide Partitioning and Transmutation*; OECD, Nuclear Energy Agency (NEA), 2011. http://www.oecd-nea.org/tools/publication?query=&div=&lang=&period=6m&sort=date&filter=1#y2011 (accessed 2012−01−27).

(4) Bell, K.; Carpentier, C.; Carrott, M.; Geist, A.; Gregson, C.; Hérès, X.; Magnusson, D.; Malmbeck, R.; McLachlan, F.; Modolo, G.; Müllmich, U.; Sypula, M.; Taylor, R.; Wilden, A. Progress Towards the Development of a New GANEX Process. *Procedia Chem.* **2012**, *7*, 392−397.

(5) Malmbeck, R.; Carrott, M.; Christiansen, B.; Geist, A.; Hérès, X.; Magnusson, D.; Modolo, G.; Sorel, C.; Taylor, R.; Wilden, A. EURO-GANEX, a Process for the Co-separation of TRU. In *Sustainable Nuclear Energy Conference*, Manchester, UK, 2014.

(6) Baron, P.; Hérès, X.; Lecomte, M.; Masson, M. Separation of the Minor Actinides: the DIAMEX-SANEX Concept. In *International Conference on Future Nuclear Systems, GLOBAL'01*, Paris, France, 2001.

(7) Wilden, A.; Modolo, G.; Geist, A. Development and demonstration of innovative partitioning processes (i-SANEX and 1-cycle SANEX) for actinide partitioning. In *13th Information Exchange Meeting on Actinide and Fission Product Partitioning and Transmutation (IEMPT13)*, OECD-NEA: Paris, 2015; Vol. NEA/NSC/R(2015)2; Seoul, Republic of Korea, September 23−26, 2014; pp 138−147.

(8) Wilden, A.; Modolo, G.; Kaufholz, P.; Sadowski, F.; Lange, S.; Munzel, D.; Geist, A. Process Development and Laboratory-scale Demonstration of a regular-SANEX Process Using C5-BPP. *Sep. Sci. Technol.* **2015**, *50* (16), 2467−2475.

(9) Wilden, A.; Sypula, M.; Schreinemachers, C.; Kluxen, P.; Modolo, G. 1-cycle SANEX process development studies performed at Forschungszentrum Jülich. In *First ACSEPT International Workshop*, Lisbon, Portugal, 2010.

(10) Sypula, M.; Wilden, A.; Schreinemachers, C.; Modolo, G. Innovative SANEX process for actinide(III) separation from PUREX raffinate using TODGA-based solvents. In *Institute of Energy and Climate Research IEK-6: Nuclear Waste Management & Reactor Safety, Report 2009/2010 − Material Science for Nuclear Waste Management*, Klinkenberg, M.; Neumeier, S.; Bosbach, D., Eds.; Vol. *119*; Forschungszentrum Jülich GmbH, 2011; pp 67−73.

(11) Wilden, A.; Sypula, M.; Schreinemachers, C.; Assenmacher, J.; Gülland, S.; Modolo, G. 1-cycle SANEX process development studies and lab-scale demonstrations for the direct recovery of trivalent actinides from PUREX raffinate. In *Institute of Energy and Climate Research IEK-6: Nuclear Waste Management & Reactor Safety, Report 2009/2010 − Material Science for Nuclear Waste Management*, Klinkenberg, M.; Neumeier, S.; Bosbach, D., Eds.; Vol. *119*; Forschungszentrum Jülich GmbH, 2011; pp 57−66.

(12) Wagner, C.; Müllich, U.; Geist, A.; Panak, P. J. Selective Extraction of Am(III) from PUREX Raffinate: The AmSel System. *Solvent Extr. Ion Exch.* **2016**, *34* (2), 103−113.

(13) Bollesteros, M.-J.; Calor, J.-N.; Costenoble, S.; Montuir, M.; Pacary, V.; Sorel, C.; Burdet, F.; Espinoux, D.; Hérès, X.; Eysseric, C. Implementation of Americium Separation from a PUREX Raffinate. *Procedia Chemistry* **2012**, *7*, 178−183.

(14) Panak, P. J.; Geist, A. Complexation and Extraction of Trivalent Actinides and Lanthanides by Triazinylpyridine N-Donor Ligands. *Chem. Rev.* **2013**, *113* (2), 1199−1236.

(15) Musikas, C.; Le Marois, G.; Fitoussi, R.; Cuillerdier, C. Properties and Uses of Nitrogen and Sulfur Donors Ligands in Actinide Separations. In *Actinide Separations, ACS Symposium Series*, Vol. *117*; American Chemical Society, 1980; pp 131−145.

(16) Wagner, C.; Mossini, E.; Macerata, E.; Mariani, M.; Arduini, A.; Casnati, A.; Geist, A.; Panak, P. J. Time-Resolved Laser Fluorescence Spectroscopy Study of the Coordination Chemistry of a Hydrophilic CHON 1,2,3-Triazol-4-yl pyridine Ligand with Cm(III) and Eu(III). *Inorg. Chem.* **2017**, *56* (4), 2135−2144.

(17) Wagner, C.; Mullich, U.; Geist, A.; Panak, P. J. TRLFS Study on the Complexation of Cm(III) and Eu(III) with SO_3-Ph-BTBP. *Dalton Transactions* **2015**, *44* (39), 17143−17151.

(18) Geist, A.; Müllich, U.; Magnusson, D.; Kaden, P.; Modolo, G.; Wilden, A.; Zevaco, T. Actinide(III)/lanthanide(III) Separation Via Selective Aqueous Complexation of Actinides(III) Using a Hydrophilic 2,6-Bis(1,2,4-Triazin-3-yl)-Pyridine in Nitric Acid. *Solvent Extr. Ion Exch.* **2012**, *30* (5), 433−444.

(19) Madic, C.; Hudson, M. J. *High-Level Liquid Waste Partitioning by Means of Completely Incinerable Extractants*; EUR 18038 EN; European Commission: Luxembourg, 1998.
(20) Whittaker, D.; Sarsfield, M.; Taylor, R.; Woodhead, D.; Taylor, K.; Carrott, M.; Mason, C.; Colledge, H.; Sanderson, R.; Keywood, B.; Bragg, A.; White, C.; Maher, C. Process flowsheet test of the i-SANEX process with CHON-compliant ligands in aqueous and organic phases. *Progress in Nuclear Energy* **2023**, *166* (10), No. 104956.
(21) Wilden, A.; Schneider, D.; Paparigas, Z.; Henkes, M.; Kreft, F.; Geist, A.; Mossini, E.; Macerata, E.; Mariani, M.; Gullo, M. C.; Casnati, A.; Modolo, G. Selective actinide(III) separation using 2,6-bis[1-(propan-1-ol)-1,2,3-triazol-4-yl]pyridine (PyTri-Diol) in the innovative-SANEX process: laboratory scale counter current centrifugal contactor demonstration. *Radiochim. Acta* **2022**, *110* (6−9), 515−525.
(22) Greif, G.; Sauerwein, F. S.; Weßling, P.; Duckworth, T. M.; Patzschke, M.; Gericke, R.; Sittel, T.; März, J.; Wilden, A.; Modolo, G.; Panak, P. J.; Roesky, P. W. 6-(6-Methyl-1,2,4,5-Tetrazine-3-yl)-2,2'-Bipyridine: A N-Donor Ligand for the Separation of Lanthanides(III) and Actinides(III). *Inorg. Chem.* **2024**, *63* (33), 15259−15269.
(23) Kolarik, Z.; Mullich, U.; Gassner, F. Selective extraction of Am(III) over Eu(III) by 2,6-ditriazolyl- and 2,6-ditriazinylpyridines. *Solvent Extr. Ion Exch.* **1999**, *17* (1), 23−32.
(24) Drew, M. G. B.; Guillaneux, D.; Hudson, M. J.; Iveson, P. B.; Russell, M. L.; Madic, C. Lanthanide(III) complexes of a highly efficient actinide(III) extracting agent - 2,6-bis(5,6-dipropyl-1,2,4-triazin-3-yl)pyridine. *Inorg. Chem. Commun.* **2001**, *4* (1), 12−15.
(25) Iveson, P. B.; Rivière, C.; Guillaneux, D.; Nierlich, M.; Thuéry, P.; Ephritikhine, M.; Madic, C. Selective complexation of uranium(III) over cerium(III) by 2,6-bis(5,6-dialkyl-1,2,4-triazin-3-yl)-pyridines:: 1H NMR and X-ray crystallography studies. *Chem. Commun.* **2001**, No. 16, 1512−1513.
(26) Boucher, C.; Drew, M. G. B.; Giddings, P.; Harwood, L. M.; Hudson, M. J.; Iveson, P. B.; Madic, C. 12-coordinate complexes formed by the early lanthanide metals with 2,6-bis(−1,2,4-triazin-3-yl)-pyridine. *Inorg. Chem. Commun.* **2002**, *5* (8), 596−599.
(27) Ionova, G.; Rabbe, C.; Guillaumont, R.; Ionov, S.; Madic, C.; Krupa, J. C.; Guillaneux, D. A donor-acceptor model of Ln(III) complexation with terdentate nitrogen planar ligands. *New J. Chem.* **2002**, *26* (2), 234−242.
(28) Berthet, J.-C.; Miquel, Y.; Iveson, P. B.; Nierlich, M.; Thuery, P.; Madic, C.; Ephritikhine, M. The affinity and selectivity of terdentate nitrogen ligands towards trivalent lanthanide and uranium ions viewed from the crystal structures of the 1 [ratio] 3 complexes. *J. Chem. Soc., Dalton Trans.* **2002**, *16*, 3265−3272.
(29) Colette, S.; Amekraz, B.; Madic, C.; Berthon, L.; Cote, G.; Moulin, C. Use of electrospray mass spectrometry (ESI-MS) for the study of europium(III) complexation with bis(dialkyltriazinyl)-pyridines and its implications in the design of new extracting agents. *Inorg. Chem.* **2002**, *41* (26), 7031−7041.
(30) Colette, S.; Amekraz, B.; Madic, C.; Berthon, L.; Cote, G.; Moulin, C. Trivalent lanthanide interactions with a terdentate bis(dialkyltriazinyl)pyridine ligand studied by electrospray ionization mass spectrometry. *Inorg. Chem.* **2003**, *42* (7), 2215−2226.
(31) Colette, S.; Amekraz, B.; Madic, C.; Berthon, L.; Cote, G.; Moulin, C. Europium(III) interaction with a polyaza-aromatic extractant studied by time-resolved laser-induced luminescence: A thermodynamical approach. *Inorg. Chem.* **2004**, *43* (21), 6745−6751.
(32) Denecke, M. A.; Rossberg, A.; Panak, P. J.; Weigl, M.; Schimmelpfennig, B.; Geist, A. Characterization and comparison of Cm(III) and Eu(III) complexed with 2,6-di(5,6-dipropyl-1,2,4-triazin-3-yl)pyridine using EXAFS, TRFLS, and quantum-chemical methods. *Inorg. Chem.* **2005**, *44* (23), 8418−8425.
(33) Drew, M. G. B.; Foreman, M. R. S.; Geist, A.; Hudson, M. J.; Marken, F.; Norman, V.; Weigl, M. Synthesis, structure, and redox states of homoleptic d-block metal complexes with bis-1,2,4-triazin-3-yl-pyridine and 1,2,4-triazin-3-yl-bipyridine extractants. *Polyhedron* **2006**, *25* (4), 888−900.
(34) Steppert, M.; Walther, C.; Geist, A.; Fanghanel, T. Direct nano ESI time-of-flight mass spectrometric investigations on lanthanide BTP complexes in the extraction-relevant diluent 1-octanol. *New J. Chem.* **2009**, *33*, 2467.
(35) Banik, N. L.; Schimmelpfennig, B.; Marquardt, C. M.; Brendebach, B.; Geist, A.; Denecke, M. A. Characterization of redox sensitive plutonium(III) complexed with alkylated 2,6-ditriazinylpyridine (BTP) in organic solution. *Dalton Transactions* **2010**, *39* (21), 5117−5122.
(36) Benay, G.; Schurhammer, R.; Wipff, G. BTP-based ligands and their complexes with Eu^{3+} at "oil"/water interfaces. A molecular dynamics study. *Phys. Chem. Chem. Phys.* **2010**, *12* (36), 11089−11102.
(37) Galan, D. M.; Nunez, A.; Mullich, U.; Cobos, J.; Geist, A. Stability and Recyclability of SO3-Ph-BTP for i-SANEX Process Development. In *International Solvent Extraction Conference*, Wurzburg, Germany, 2014.
(38) Peterman, D.; Geist, A.; Mincher, B.; Modolo, G.; Galán, M. H.; Olson, L.; McDowell, R. Performance of an i-SANEX System Based on a Water-Soluble BTP under Continuous Irradiation in a γ-Radiolysis Test Loop. *Ind. Eng. Chem. Res.* **2016**, *55* (39), 10427−10435.
(39) Horne, G. P.; Mezyk, S. P.; Moulton, N.; Peller, J. R.; Geist, A. Time-resolved and steady-state irradiation of hydrophilic sulfonated bis-triazinyl-(bi)pyridines - modelling radiolytic degradation. *Dalton Trans.* **2019**, *48* (14), 4547−4554.
(40) Buxton, G. V.; Greenstock, C. L.; Helman, W. P.; Ross, A. B. Critical-review of rate constants for reactions of hydrated electrons, hydrogen-atoms and hydroxyl radicals (.OH/.O-) in aqueous-solution. *J. Phys. Chem. Ref. Data* **1988**, *17* (2), 513−886.
(41) Katsumura, Y. NO_2 and NO_3 Radicals in the Radiolysis of Nitric Acid Solutions. In *The Chemistry of Free Radicals: N-Centered Radicals*, Alfassi, Z. B., Ed.; John Wiley & Sons, The Chemistry of Free Radicals, 1998; pp 393−412.
(42) Davis, W., Jr.; De Bruin, H. J. New Activity Coefficients of 1−100% Aqueous Nitric Acid. *Journal of Inorganic & Nuclear Chemistry* **1964**, *26* (6), 1069−1083.
(43) Ruas, A.; Pochon, P.; Simonin, J. P.; Moisy, P. Nitric acid: modeling osmotic coefficients and acid-base dissociation using the BIMSA theory. *Dalton Trans.* **2010**, *39* (42), 10148−10153.
(44) Hlushak, S.; Simonin, J. P.; De Sio, S.; Bernard, O.; Ruas, A.; Pochon, P.; Jan, S.; Moisy, P. Speciation in aqueous solutions of nitric acid. *Dalton Trans.* **2013**, *42* (8), 2853−2860.
(45) Mezyk, S. P.; Bartels, D. M. Temperature dependence of hydrogen atom reaction with nitrate and nitrite species in aqueous solution. *J. Phys. Chem. A* **1997**, *101* (35), 6233−6237.
(46) Garaix, G.; Horne, G. P.; Venault, L.; Moisy, P.; Pimblott, S. M.; Marignier, J. L.; Mostafavi, M. Decay Mechanism of $NO_3^{\bullet}$ Radical in Highly Concentrated Nitrate and Nitric Acidic Solutions in the Absence and Presence of Hydrazine. *J. Phys. Chem. B* **2016**, *120* (22), 5008−5014.
(47) Jiang, P. Y.; Katsumura, Y.; Ishigure, K.; Yoshida, Y. Reduction Potential of the Nitrate Radical In Aqueous-Solution. *Inorg. Chem.* **1992**, *31* (24), 5135−5136.
(48) Kynman, A. E.; Grimes, T. S.; Cook, A. R.; Peterman, D. R.; Horne, G. P. Influence of americium complexation on the radiation-induced chemical reactivity of sulfophenyl bistriazinyl pyridine (SO3-Ph-BTP) towards the nitrate radical. *Radiat. Phys. Chem.* **2025**, *239*, No. 113246.
(49) Collins, R. N.; Saito, T.; Aoyagi, N.; Payne, T. E.; Kimura, T.; Waite, T. D. Applications of Time-Resolved Laser Fluorescence Spectroscopy to the Environmental Biogeochemistry of Actinides. *J. Environ. Qual.* **2011**, *40* (3), 731−741.
(50) Ruff, C. *Spektroskopische und thermodynamische Untersuchung der Komplexierung von Cm(III) und Eu(III) mit hydrophilen Bis-Triazinylpyridinen*. Ruprecht-Karls-Universität Heidelberg, 2013.
(51) Turanov, A. N.; Karandashev, V. K. Synergistic Extraction of U(VI), Th(IV), and Lanthanides(III) from Nitric Acid Solutions

https://doi.org/10.1021/acs.iecr.5c04766
Ind. Eng. Chem. Res. 2026, 65, 6127−6142

Using Mixtures of TODGA and Dinonylnaphthalene Sulfonic Acid. *Solvent Extr. Ion Exch.* **2018**, *36*, 257.
(52) Xiao, C. L.; Wang, C. Z.; Yuan, L. Y.; Li, B.; He, H.; Wang, S.; Zhao, Y. L.; Chai, Z. F.; Shi, W. Q. Excellent Selectivity for Actinides with a Tetradentate 2,9-Diamide-1,10-Phenanthroline Ligand in Highly Acidic Solution: A Hard-Soft Donor Combined Strategy. *Inorg. Chem.* **2014**, *53* (3), 1712−1720.
(53) Tang, Y. Q.; Weng, N. D. Salting-out assisted liquid-liquid extraction for bioanalysis. *Bioanalysis* **2013**, *5* (12), 1583−1598.
(54) Hyde, A. M.; Zultanski, S. L.; Waldman, J. H.; Zhong, Y. L.; Shevlin, M.; Peng, F. General Principles and Strategies for Salting-Out Informed by the Hofmeister Series. *Org. Process Res. Dev.* **2017**, *21* (9), 1355−1370.
(55) Allahkarami, E.; Rezai, B.; Bozorgmehr, M.; Adib, S. Extraction of neodymium(III) from aqueous solutions by solvent extraction with Cyanex® 572. *Physicochem. Probl. Mineral Pro.* **2021**, *57* (3), 127−135.
(56) Ruff, C. M.; Müllich, U.; Geist, A.; Panak, P. J. A novel path in partitioning: Water-soluble BTP ligands for the innovative SANEX process. *Atw, Int. J. Nucl. Power* **2011**, *56* (8−9), 489−491.
(57) Arisaka, M.; Kimura, T. Thermodynamic and Spectroscopic Studies on Am(III) and Eu(III) in the Extraction System of N,N,N',N'-Tetraoctyl-3-Oxapentane-1,5-Diamide in n-Dodecane/Nitric Acid. *Solvent Extr. Ion Exch.* **2011**, *29* (1), 72−85.
(58) Weßling, P.; Trumm, M.; Geist, A.; Panak, P. J. Stoichiometry of An(III)−DMDOHEMA complexes formed during solvent extraction. *Dalton Transactions* **2018**, *47* (32), 10906−10914.
(59) Ruff, C. M.; Müllich, U.; Geist, A.; Panak, P. J. Complexation of Cm(III) and Eu(III) with a hydrophilic 2,6-bis(1,2,4-triazin-3-yl)-pyridine studied by time-resolved laser fluorescence spectroscopy. *Dalton Transactions* **2012**, *41* (48), 14594−14602.
(60) Wilden, A.; Modolo, G.; Lange, S.; Sadowski, F.; Beele, B. B.; Skerencak-Frech, A.; Panak, P. J.; Iqbal, M.; Verboom, W.; Geist, A.; Bosbach, D. Modified Diglycolamides for the An(III) + Ln(III) Co-separation: Evaluation by Solvent Extraction and Time-Resolved Laser Fluorescence Spectroscopy. *Solvent Extr. Ion Exch.* **2014**, *32* (2), 119−137.
(61) Wilden, A.; Modolo, G.; Lange, S.; Sadowski, F.; Beele, B. B.; Skerencak-Frech, A.; Panak, P. J.; Geist, A.; Iqbal, M.; Verboom, W.; Bosbach, D. Modified Diglycolamides for Actinide Separation: Solvent Extraction and Time Resolved Laser Fluorescence Spectroscopy Complexation Studies. In *GLOBAL 2013 "Nuclear Energy at a Crossroad"*, Salt Lake City, UT, USA, 2013; pp 907−911.
(62) Whitman, K. L. S.; Miller, R.; Nett, D.; Treas, P.; Zante, A.; Fessenden, R. W.; Thomas, M. D.; Wang, Y. In Linear accelerator for radiation chemistry research at Notre Dame 1995. *In 95' Particle Accelerator Conference and International Conference of High Energy Accelerators*, Dallas, Texas, USA, 1996.
(63) Hug, G. L.; Wang, Y. C.; Schoneich, C.; Jiang, P. Y.; Fessenden, R. W. Multiple time scales in pulse radiolysis. Application to bromide solutions and dipeptides. *Radiat. Phys. Chem.* **1999**, *54* (6), 559−566.
(64) Cercek, B. Activation Energies for Reactions of Hydrated Electron. *Nature* **1969**, *223* (5205), 491.
(65) Varghese, R.; Mohan, H.; Manoj, P.; Manoj, V. M.; Aravind, U. K.; Vandana, K.; Aravindakumar, C. T. Reactions of hydrated electrons with triazine derivatives in aqueous medium. *J. Agric. Food Chem.* **2006**, *54* (21), 8171−8176.
(66) Neta, P.; Schuler, R. H. Rate Constants for Reaction of Hydrogen - Atoms with Aromatic and Heterocyclic Compounds - Electrophilic Nature of Hydrogen Atoms. *J. Am. Chem. Soc.* **1972**, *94* (4), 1056.
(67) Hansch, C.; Leo, A.; Taft, R. W. A Survey of Hammett Substituent Constants and Resonance and Field Parameters. *Chem. Rev.* **1991**, *91* (2), 165−195.

https://doi.org/10.1021/acs.iecr.5c04766
Ind. Eng. Chem. Res. 2026, 65, 6127−6142